

Molecular insights into RNA recognition and gene regulation by the TRIM-NHL protein Mei-P26

Anna Salerno-Kochan^{1,2}, Andreas Horn³, Pritha Ghosh⁴, Chandran Nithin^{4,*}, Anna Kościelniak¹, Daniela Strauss³, Oliver Rossbach⁵, Janusz M. Bujnicki^{4,6}, Monika Gaik^{1,#}, Jan Medenbach^{3,#} and Sebastian Glatt^{1,#}

¹ Malopolska Centre of Biotechnology, Jagiellonian University Krakow, Poland

² Postgraduate School of Molecular Medicine, Warsaw, Poland

³ Biochemistry I, University of Regensburg, Germany

⁴ Laboratory of Bioinformatics and Protein Engineering, International Institute of Molecular and Cell Biology in Warsaw, Poland

⁵ Institute of Biochemistry, University of Giessen, Germany

⁶ Bioinformatics Laboratory, Institute of Molecular Biology and Biotechnology, Faculty of Biology, Adam Mickiewicz University, Poznan, Poland

* Present address: Laboratory of Computational Biology, Faculty of Chemistry, Biological and Chemical Research Centre, University of Warsaw, Warsaw 02-089, Poland

Correspondence to MG (monika.gaik@uj.edu.pl), JM (Jan.Medenbach@vkl.uni-regensburg.de) and SG (sebastian.glatt@uj.edu.pl)

Keywords: Mei-P26, NHL, RNA recognition, TRIM-NHL proteins, stem cell differentiation, translational regulation

Running title: Structural and functional characterization of the Mei-P26 NHL domain

1 **Abstract**

2 The TRIM-NHL protein Meiotic P26 (Mei-P26) acts as a regulator of cell fate in
3 *Drosophila*. Its activity is critical for ovarian germline stem cell maintenance, differentiation
4 of oocytes and spermatogenesis. Mei-P26 functions as a post-transcriptional regulator of gene
5 expression, however, the molecular details of how its NHL domain selectively recognizes and
6 regulates its mRNA targets have remained elusive. Here, we present the crystal structure of
7 the Mei-P26 NHL domain at 1.6 Å resolution and identify key amino acids that confer
8 substrate specificity and distinguish Mei-P26 from closely related TRIM-NHL proteins.
9 Furthermore, we identify mRNA targets of Mei-P26 in cultured *Drosophila* cells and show
10 that Mei-P26 can act as either a repressor or activator of gene expression on different RNA
11 targets. Our work reveals the molecular basis of RNA recognition by Mei-P26 and the
12 fundamental functional differences between otherwise very similar TRIM-NHL proteins.

13 Introduction

14 RNA binding proteins (RBPs) play key roles in the post-transcriptional regulation of
15 gene expression. They comprise a large and functionally diverse group of proteins involved in
16 all aspects of RNA biology from RNA synthesis to its degradation. RBPs typically bind
17 RNAs through dedicated RNA-binding domains (RBDs)(1). Several members of the
18 evolutionary conserved TRIM-NHL family employ their NHL domains to interact with RNA
19 (2–6). The TRIM-NHL protein family shares a common architecture comprised of an N-
20 terminal tripartite motif (TRIM, consisting of a RING domain, one or two B-Box type zinc
21 fingers and a coiled-coil domain) followed by a C-terminal NCL-1, HT2A, LIN-41 (NHL)
22 domain (7–11). The NHL domain folds into a β -propeller that typically acts as a scaffold to
23 mediate interactions with other biomolecules such as proteins, DNA or RNA (6, 12, 13).

24 TRIM-NHL proteins play important roles in development where they control cell fate
25 decisions to regulate differentiation and cell growth (11, 14). The *Drosophila melanogaster*
26 genome encodes several proteins with a TRIM-NHL-like architecture, among them Brain
27 tumor (Brat) and Meiotic-P26 (Mei-P26). Mei-P26 was identified as a regulator of
28 differentiation in the male and female germline and its loss results in over-proliferation of
29 germline cells, tumor formation and sterility (15–19). Germline homeostasis depends on the
30 maintenance of germline stem cells (GSCs) in the stem cell niche and on the proper
31 differentiation of their progeny into gametes (20). In the female germline, Mei-P26 supports
32 both cellular programs. It ensures maintenance of GSCs through control of BMP signaling
33 (17), but also promotes differentiation of daughter cells upon exit from the stem cell niche
34 (18). In the male germline, Mei-P26 limits mitotic divisions during the differentiation process
35 of precursor germ cells preventing over-proliferation (16). Moreover, ovarian cells lacking
36 Mei-P26 activity grow abnormally large and exhibit increased nucleolar size (21).

37 The function of the closely-related Brat protein critically depends on its NHL domain
38 as its deletion or other sequence alterations result in strong phenotypes that can be partially
39 rescued by expression of the NHL domain alone (22, 23). The Brat NHL domain participates
40 in multiple protein-protein interactions involving factors such as Pum, eIF4EHP and Miranda
41 as binding partners (23–28). Similarly, Mei-P26 function requires several additional proteins,
42 among them, Sxl (Sex-lethal), Bam (Bag of marbles), Bgcn (Benign gonial cell neoplasm),
43 Wuho and Ago1 (Argonaute-1) (17, 21, 29, 30). The Mei-P26 NHL domain is required for the
44 interaction with at least some of these proteins, as mutations leading to substitutions in its
45 sequence abolish the interaction with Ago1 and impair ovarian stem cell maintenance (21).
46 Finally, the NHL domains of both Brat and Mei-P26 interact with RNA in a sequence-specific
47 manner (3, 6, 31).

48 Considering the functional importance of the Mei-P26 NHL domain, we conducted
49 comprehensive structural and functional analyses. We confirm the high structural similarity
50 between the NHL domains of Mei-P26 and Brat, but also detect subtle differences that
51 influence their function and affect target specificity. Computational modeling of the Mei-P26
52 NHL interaction with its RNA substrate allowed us to predict and experimentally validate key
53 residues critical for sequence-specific RNA binding. Finally, we employed individual-
54 nucleotide resolution cross-linking and immunoprecipitation (iCLIP) to identify cellular
55 mRNA targets of full-length Mei-P26 and its NHL domain. We confirm the recognition of
56 several identified target sequences by Mei-P26 using individual EMSA analyses.
57 Furthermore, we show that Mei-P26 directly affects the expression of reporters that carry
58 these newly identified Mei-P26 binding sites and dissect the domain requirements for
59 regulation. In summary, our results deepen the molecular understanding of NHL-RNA
60 interactions that play a key function in governing cell fate decisions.

61

62 **Materials and Methods**

63 **DNA constructs**

64 First, the coding sequence of Mei-P26 NHL (isoform C/E) was amplified by RT-PCR
65 from total RNA (prepared from *Drosophila* embryos, strain Oregon-R) and cloned into a
66 modified pFastBac HTA vector carrying an additional N-terminal GST tag sequence followed
67 by a TEV cleavage site. Mutated variants of Mei-P26 NHL were obtained using the
68 QuickChange cloning protocol. For Brat-NHL, the His6-ubiquitin fusion protein produced
69 from the pHUE vector was used (a gift from I. Loedige) (6). For the luciferase reporter
70 plasmids, 3' UTR fragments of select genes were RT-PCR amplified from total RNA prepared
71 from *Drosophila* S2R+ cells (primers and RNA regions are provided in supplementary table
72 1) and ligated into a modified pCasPeR-Heatshock vector containing a Firefly luciferase open
73 reading frame (pHS-FLuc (32)) using the *HpaI* and *BglII* restriction sites. A vector encoding
74 Renilla luciferase (pHS-B_m-RLuc-(EF)m-SV40 aka pHS-RL) (32) was used for co-
75 transfection and served as a reference for normalization. Plasmids encoding HA-tagged or
76 lambda N-HA-tagged, full-length Mei-P26 or Brat were kindly provided by I. Loedige (MDC
77 Berlin) and G. Meister (University of Regensburg). For iCLIP experiments, the coding
78 sequences of Mei-P26 and its NHL domain were subcloned into a modified pAc5.1 vector
79 using the *SbfI* and *NotI* restriction sites to generate expression plasmids encoding N-
80 terminally 2x FLAG-tagged proteins. Point mutations in the NHL domain were subsequently
81 introduced using site-directed mutagenesis. The sequences of all oligonucleotides used for
82 cloning are provided in the table (see **Supplementary Table 1**). All vectors were validated by
83 sequencing.

84 **Protein expression and purification**

85 Mei-P26 NHL and its mutated variants were obtained using Bac-to-Bac baculovirus
86 expression system according to standard protocols. For protein expression, Hi5 insect cells

87 were infected at a MOI of 0.5 and grown for 3 days at 27°C. After harvesting (4°C, 15', 7 000
88 rcf), the cell pellets were resuspended in lysis buffer (50 mM HEPES pH 7.5, 600 mM NaCl,
89 10% Glycerol, 5 mM MgCl₂, 1 mM DTT, DNase), snap frozen in liquid nitrogen and stored
90 in -80°C. For purification, cells were lysed by 3 cycles of freezing and thawing, followed by
91 mild sonication and centrifugation (4°C, 1h, 80 000 rcf). The supernatant was applied and
92 circulated on a Glutathione Sepharose 4 Fast Flow 16/10 column (GE Healthcare) for 16 h,
93 then washed with buffer A (50 mM HEPES pH 7.5, 600 mM NaCl, 10% Glycerol, 1 mM
94 DTT) and high salt buffer A (50 mM HEPES pH 7.5, 1 M NaCl, 10% Glycerol, 1 mM DTT).
95 Elution occurred in a buffer containing 50 mM HEPES pH 8, 600 mM NaCl, 1 mM DTT, 10
96 mM Glutathione. The elution fractions were pooled, supplemented with TEV protease and
97 dialysed overnight against the dialysis buffer (20 mM HEPES, 300 mM NaCl, 1 mM DTT).
98 Subsequently, the samples were re-adsorbed onto a Glutathione Sepharose 4 Fast Flow 16/10
99 column (GE Healthcare) and the flow-through was purified by size exclusion chromatography
100 using a Superdex 200 10/300 GL column (GE Healthcare). Purified samples were stored in
101 gel filtration buffer (20 mM HEPES, 300 mM NaCl, 5 mM DTT). Brat-NHL was expressed
102 and purified as previously described (31).

103 **Crystallization and structure determination**

104 Mei-P26 NHL crystals were grown at 20°C using the sitting drop vapor diffusion
105 method. The purified protein was concentrated to 11 mg/ml in gel filtration buffer and
106 combined with an equal volume of reservoir solution (0.2 Potassium thiocyanate and 20%
107 PEG3350). After 2 weeks of incubation, crystals were fished, cryo-protected with 30%
108 glycerol and subsequently frozen in liquid nitrogen. Datasets were collected at BESSY II
109 Helmholtz-Zentrum Berlin beamlines 14.1 and 14.2. Data processing was performed using
110 XDS (33) and initial phases were obtained by molecular replacement using a search poly-
111 alanine model based of Brat-NHL (PDB code 1Q7F) (28) in Phaser (34). A structure model

112 was built in COOT (35) and subsequently refined in Phenix (36). All dataset and refinement
113 statistics are given in table (**Table 1**). Model figures were generated using Pymol (37).

114 **RNAcompete analysis**

115 RNAcompete data for the Brat and Mei-P26 NHL domains were obtained from Prof.
116 Timothy Hughes' laboratory at the University of Toronto (6). The raw data was
117 computationally split into two halves (Set A and B) in the RNAcompete pipeline (38) to
118 facilitate internal data comparisons. Next, the Z-scores for 7-mers for Set A, Set B and the
119 average of Set A and Set B (Set A+B) were calculated, ranked and presented on scatter plots.
120 Consensus motifs recognized by Mei-P26 and Brat were calculated from average of two
121 halves of the RNA pool.

122 **Modelling of Mei-P26-NHL:RNA complexes**

123 The initial structure of the Mei-P26-NHL:RNA complex was generated by
124 superimposing the Mei-P26 protein with the Brat-RNA complex (PDB ID: 5EX7) and
125 copying the coordinates of the Brat RNA ligand. The superposition was performed for the 257
126 C α atoms (RMSD = 1.343 Å), which matches between the Mei-26-NHL and Brat proteins.
127 The sequence of that RNA was modified to UUUUUUU, UUUUACA, or UUUGUUGU
128 using UCSF Chimera (39) to prepare three starting structures for Mei-P26-NHL:RNA
129 complexes. Molecular dynamics simulations for Mei-P26-NHL:RNA complexes for the three
130 cases were performed using the Amber18 package (40). Molecular dynamics simulations
131 were run for Brat in complex with UUGUAAA, UUUUACA and UUGUUGU RNAs as
132 controls. The input structure for the simulation was prepared using tleap in a truncated
133 octahedral box of 10 Å allowance using the TIP3P water model (41). Simulations were
134 performed using the combination of the Amber ff14sb force field for proteins (42) and the
135 χ OL3 force field for RNA (43, 44). The structure was energy-minimized for 10,000 cycles
136 with restraints, followed by 10,000 cycles without restraints. The minimized structures were

137 subjected to heating, density equilibration and short runs of equilibration. The heating was
138 done from 100 K to 300 K for 500 ps with restraints on the entire structure and the density
139 equilibration was performed for 500 ps, also with restraints on the entire structure. The
140 equilibration of the structures was run for four short rounds. The first three rounds of
141 equilibration were run for 200 ps each with the main chain atoms constrained. The final round
142 of equilibration was performed for 2 ns to ensure full convergence and reliability of the
143 models. The production run was run for 1 μ s. We have used constant pressure periodic
144 boundary conditions (ntb = 2) with isotropic position scaling (ntp = 1) with a pressure
145 relaxation time $\tau_{\text{p}} = 2.0$ ps for the production run. The particle-mesh Ewald (PME)
146 procedure (45) was used for computing the electrostatic interactions. The cut-off values used
147 for electrostatics and LJ interactions were set as 12 Å. The equilibration steps were run with
148 the NVT ensemble (ntb = 1) while the production run was performed with the NPT ensemble.
149 The minimization was performed using Sander and the subsequent steps were performed
150 using the CUDA version of PMEMD available in the Amber package (46–48). The simulation
151 trajectories were clustered using the reimplementation of NMRCLUST algorithm (49)
152 available in UCSF Chimera and the representative frames (**Supplementary Fig. 4, 5**) are
153 provided as PDB files in the supplementary materials. All simulated models and the used
154 restraints were deposited to a publicly available data repository (Mendeley Data;
155 doi:10.17632/jvkcwfyz47.1). The Theseus analysis was performed to evaluate the MD
156 simulation by simultaneous superposition of the Brat NHL - UUGUUGU crystal structure
157 (PDB ID: 5EX7) with the Brat NHL - UUGUUGU model and the top five clusters from
158 representative models (52).

159 **Microscale thermophoresis**

160 Experiments were conducted using 20 nM of Cy5-labeled oligonucleotides in the
161 buffer containing 20 mM HEPES, 100 mM NaCl, 5 mM MgCl_2 , 5 mM DTT, 0.0125% Tween

162 20 for Mei-P26 NHL and 20 mM Tris 8.0, 150 mM NaCl, 1 mM MgCl₂, 5 mM DTT,
163 0.0125% Tween 20 for Brat NHL. 3:1 serial dilutions of unlabelled protein (starting from the
164 highest concentration of 5 μM) was mixed with labelled oligonucleotide, incubated for 15
165 minutes and applied for measurements. Measurements were conducted at 40% MST power
166 and light-emitting diode (LED)/excitation power setting 20% in Premium Coated capillaries
167 on the Monolith NT.115 at 25°C (Nanotemper Technologies). Each experiment was
168 performed in at least three replicates. The data were analysed using the MO.Affinity software
169 (Nanotemper Technologies) at the standard MST on time off 5 s. To calculate dissociation
170 constants (K_d), Hill models were fitted to each dataset. The graphs were prepared in GraphPad
171 Prism software. Oligonucleotides used in the experiments are listed in **Supplementary Table**
172 **1**.

173 **Electromobility shift assays (EMSA)**

174 15 pmol of RNA/DNA were radioactively labeled for 1 h at 37 °C using 5 U T4
175 Polynucleotide Kinase (Thermo Fisher) and 10 μCi γ-³²P ATP. The reaction was inactivated
176 at 75 °C for 10 min and the labeled RNA/DNA was purified by gel filtration (Illustra
177 MicroSpin G-25 columns; GE Healthcare). Recombinant, wild-type Mei-P26 NHL was
178 prepared in 20 mM HEPES/KOH pH 7.5, 100 mM NaCl, 5 mM DTT, 5% glycerol, variants
179 were prepared in the same buffer but containing 300 mM NaCl. 10 fmol of RNA/DNA were
180 diluted in 10 mM Tris/Cl pH 7.4, 50 mM KCl, 1mM EDTA, 1 mM DTT, 0.4 mg/ml yeast
181 tRNA (Invitrogen) and mixed with the indicated amounts of recombinant protein in a total
182 reaction volume of 10 μl. After incubation for 30 min at 4°C, samples were separated by
183 electrophoresis (6% polyacrylamide [37.5:1 acrylamide:bisacrylamide], 5% glycerol,
184 44.5 mM Tris, 44.5 mM boric acid) at 230 V for 60 min at 4 °C. Gels were dried for 2 h at 80
185 °C and analysed on a Personal Molecular Imager (Bio-Rad). For RNA stability assays, 10 μl
186 reactions were set up as described above, containing radioactively labeled RNA and 1280 nM

187 of the purified NHL domain. Control reactions were supplemented with buffer instead of the
188 protein preparation. After 30 minutes of incubation at 4°C, RNAs were purified by organic
189 extraction, separated by 15% denaturing PAGE and visualized by autoradiography.

190 **Thermal shift assays**

191 Recombinant Mei-P26 NHL domain and variants thereof (each at a concentration of
192 1g/l) were incubated with SYPRO Orange and 20 mM HEPES pH 7.5, 300 mM NaCl, 5 mM
193 DTT buffer in 96-well plates followed by centrifugation (5', 1000 rpm). Subsequently, the
194 samples were gradually heated from 4 to 98°C with a rate of 0.2°C/10 s in the CFX96 Real-
195 Time System C1000 Touch Thermal Cycler (Biorad). The fluorescence intensity was
196 measured using an excitation wavelength of 470 nm while monitoring emission at 570 nm.

197 **Tissue culture**

198 *Drosophila* S2R+ cells were propagated at 25°C at 80% confluency in Express Five
199 SFM supplemented with 10X Glutamax (Thermo Fisher).

200 **Western blotting**

201 Cultured cells were harvested and resuspended in lysis buffer (20 mM Tris/Cl pH 8.0,
202 150 mM NaCl, 5 mM EDTA, 1% NP-40, 2% SDS). Protein concentration of cleared lysates
203 was determined using the BioRad protein assay reagent. 25 µg of total protein were separated
204 by denaturing PAGE and subjected to Western blotting using mouse monoclonal anti-FLAG
205 antibody (M2, Sigma Aldrich, 1:1000) followed by probing with an HRP-coupled anti-mouse
206 light chain-specific secondary antibody (1:10000, Jackson Immuno Research). Detection
207 occurred by using Clarity Western ECL substrate and a ChemiDoc Touch Imaging System
208 (BioRad). After stripping, the membrane was re-probed using mouse anti-alpha-tubulin
209 antibody (DM1A, Sigma Aldrich, 1:1000).

210 **Individual-nucleotide cross-linking and immunoprecipitation (iCLIP)**

211 Cells were transfected for 48 h with 15 µg DNA per 15 cm dish using Fugene HD
212 (Promega) following the manufacturer's instructions using plasmids encoding full-length
213 FLAG-tagged MeiP26 protein, its NHL domain only, or their respective mutant versions. A
214 novel, improved version of the iCLIP method was utilized, termed "iCLIP2" (53). Briefly, a
215 15-cm dish of cells was washed with PBS and UV-irradiated (120mJ/cm² at 254 nm) using a
216 UV Stratalinker 2400 (Stratagene). Next, cell extract was prepared and subjected to RNase
217 treatment using 10 U of RNase I (Ambion). Immunoprecipitation was performed with anti-
218 FLAG antibody (M2, Sigma Aldrich) or control serum on Dynabeads Protein A (Life
219 Technologies) for 2 h at 4°C. After washing four times with washing buffer (50 mM Tris/Cl
220 pH 7.4, 1 M NaCl, 0.05% Tween 20), the co-immunoprecipitated RNA was
221 dephosphorylated, ligated to a 3'-RNA linker and 5'-radiolabeled with T4 PNK and [γ -³²P]-
222 ATP. Samples were subjected to neutral SDS-PAGE (NuPAGE, Invitrogen) and transferred to
223 a nitrocellulose membrane. Protein/RNA-complexes were visualized by autoradiography.
224 Mei-P26:RNA-complexes were cut from the membrane, proteins were digested with
225 Proteinase K and RNA was subjected to iCLIP2 library preparation as previously described
226 (53). Sequencing occurred on a HiSeq 2500 (Illumina). Three independent biological
227 replicates were performed for each protein construct; as a control, non-transfected cells were
228 processed in parallel.

229 **iCLIP data analysis**

230 The iCLIP data were processed using the iCount software suite and analysis pipeline
231 (54). The sequencing reads were demultiplexed based on barcodes for individual replicates
232 (allowing one mismatch), PCR duplicates were removed and adapters were trimmed. The
233 reads for each of the replicates were aligned to the *Drosophila melanogaster* genome
234 (ENSEMBL release 98) and processed separately. Cross-linked nucleotides (peaks) were
235 identified and then clustered. Gene loci that produced iCLIP peaks in the experiments

236 conducted with both, the full-length protein and the NHL domain were manually curated.
237 When crosslinking occurred to mitochondrially-encoded RNAs (4 loci in total) or known
238 contaminants such as snoRNA/scaRNA/snRNA sequences (or similar) present in the host
239 genes (17 loci), the gene loci were excluded from further analyses. Similarly, crosslinking to
240 low complexity regions (mostly A-stretches that resemble polyA-tails) or sequences derived
241 from the transfected plasmids (originating from the Actin5C promoter or the Mei-P26 coding
242 region) were not considered. In the remaining 214 genes, crosslinking positions were
243 considered equivalent between the individual experiments when the distance between the
244 crosslinking peaks (full-length versus NHL domain) was <50 nt. In these loci, the presence of
245 Mei-P26 RNA target motifs was scored up to 30 nt upstream and 20 nt downstream of the
246 crosslink positions, considering full matches (UUUUACN, UUUUANA, UUUUNCA, or
247 UUUUUUU, 65 loci) or U-rich sequences with four consecutive U residues followed by 3 nt
248 containing at least one additional U residue (63 loci).

249 **Tethering- and reporter assays**

250 For tethering assays, per well of a 96-well plate 4×10^4 *Drosophila* SR2+ cells were
251 seeded and transfected using Fugene (Promega) according to the manufacturer's instructions
252 with the following plasmids: (1) 10 ng of a Firefly luciferase reporter with five BoxB
253 elements in the 3' UTR (pAC-FL-5boxB, kindly provided by I. Loedige), (2) 30 ng of a
254 control plasmid encoding Renilla luciferase and (3) 60 ng of plasmids encoding either HA- or
255 λ NHA-tagged proteins of interest. 48 h after transfection, the cells were lysed with 1x Passive
256 Lysis Buffer (Promega) and luciferase activities were determined using the Dual-Luciferase
257 Reporter Assay System (Promega) and a Centro LB 960 luminometer (Berthold). Relative
258 luciferase units (RLUs) were calculated for each sample by dividing Firefly luciferase activity
259 by Renilla luciferase activity. Activities are expressed as the ratio of RLUs obtained for the
260 tethered, λ NHA-tagged proteins relative to the untethered control proteins. Depicted are mean

261 values \pm standard deviation of at least three independent biological experiments performed in
262 technical triplicates. 3' UTR reporter assays were performed analogously. The transfection
263 mixture contained 100 ng of plasmid DNA consisting of 23.3 ng Firefly luciferase reporter
264 plasmid (pHS-FL bearing different 3' UTR sequences), 1.7 ng Renilla luciferase encoding
265 plasmid (pHS-RL, normalization control) and 75 ng of a pAc5.1 plasmid encoding either
266 2xFLAG-tagged Mei-P26, or a mutant version thereof. An empty pAc5.1 plasmid served as a
267 control. 48 h after transfection, RLU were determined as described above and normalized to
268 the empty pAc5.1 vector control. Depicted are mean values \pm standard deviation of at least
269 three independent biological experiments performed in technical triplicates.

270 **Results**

271 **The crystal structure of the *Drosophila* Mei-P26 NHL domain**

272 To gain molecular insight into RNA binding of *Drosophila melanogaster* Mei-P26, we
273 aimed to obtain structural information of its C-terminal NHL domain (Mei-P26 NHL) at high
274 resolution. Therefore, we predicted the beginning of the NHL domain and expressed different
275 constructs using a baculovirus expression system. We obtained large quantities of Mei-P26
276 NHL_{aa908-1206} producing a homogenous monomer of approximately 30 kDa, which was
277 completely free of any proteinaceous contaminants and nucleic acids (**Fig. 1A**). Mei-P26
278 NHL crystallized in several tested conditions and we collected numerous complete datasets at
279 various synchrotron sources. We solved the structure of the Mei-P26 NHL domain at 1.6 Å
280 resolution by molecular replacement using the backbone of the previously determined Brat
281 NHL domain (28) as a reference model. The N-terminus of the NHL domain remains invisible
282 due to averaging of its conformations throughout the crystal but is present as there was no
283 indication of proteolytic degradation during purification and crystallization (**Supplementary**
284 **Fig. 1A, B**). After refinement, an atomic model could be obtained with R/R_{free} values of

285 20.6%/21.9% obeying all basic rules of protein stereochemistry (**Table 1**). Mei-P26 NHL
286 folds into a six-bladed β -propeller with a donut-like shape and a diameter of ~ 45 Å and a
287 height of ~ 25 Å (**Fig. 1A**). The two molecules located in the asymmetric unit are connected
288 by a di-sulfide bond between Cys1030, but the functional relevance of this dimerization under
289 reducing conditions *in vivo* remains questionable. The six blades are asymmetrically
290 distributed in a radial fashion around a central axis. Each unit is composed of four antiparallel
291 β -strands connected by loops of various length and degrees of flexibility. In the center of the
292 molecule the six β -sheets form a solvent channel with a diameter of approximately 12 Å. The
293 overall structure is stabilized by a β -sheet complementation of the first N-terminal β -strand
294 (aa 933-940) with the sixth sheet (aa 1178-1202) in a molecular velcro-like fashion.

295 **Mei-P26 NHL binds to single-stranded RNA**

296 We compared the structure of Mei-P26 NHL to the NHL domains of Brat, Lin41 and
297 Thin/Abba to gain further insights into their unique and commonly shared features (3, 31, 55).
298 All four proteins act as post-transcriptional repressors of gene expression and recognize their
299 target RNAs via their NHL domains. Recently, the RNA binding modes for Brat and Lin41
300 have been reported, highlighting the existence of two distinct recognition mechanisms. In
301 detail, the NHL domain of Brat binds to linear single-stranded RNA motifs (6), while the
302 NHL domain of Lin41 prefers RNA hairpins (3). The NHL domains of the *D. melanogaster*
303 Mei-P26 and Brat are closely related to each other, whereas the NHL domain of Lin41 from
304 *D. rerio* noticeably resembles the NHL domains of the fly Wech and human TRIM71 proteins
305 (3, 6). Thin/Abba is a member of a distinct branch of the TRIM-NHL phylogeny, which also
306 includes *H. sapiens* TRIM32 and *C. elegans* NHL-1 (14). These evolutionary relationships are
307 also observed on the structural level, although all four NHL domains in principle share a
308 similar overall architecture and differ only in the length of individual loops and β -strands
309 (**Supplementary Fig. 1C**). As with Brat and Lin41, the NHL domain of Mei-P26 and

310 Thin/Abba also exhibit a highly positively charged patch on their top surface
311 (**Supplementary Fig. 1D**) (3, 31, 55, 56). Because it has been experimentally demonstrated
312 that RNA binding in NHL domains occurs via this charged surface area, it was previously
313 assumed that Mei-P26 NHL can also bind to RNA (3, 6, 31). However, 11 out of 15 of the
314 residues important for RNA binding in the closely related Brat NHL domain are not
315 conserved in the Mei-P26 NHL domain (**Supplementary Fig. 1E, Supplementary Fig. 2**).
316 There is, however, one notable exception: three amino acids important for the recognition of
317 the first position of the RNA target by Brat (a uridine base interacting with Asn800, Tyr829
318 and Arg847) are conserved in Mei-P26 (Asn970, Tyr 999 and Arg1017). This suggests that
319 Mei-P26 also binds a uridine base in the same region but utilizes varying, non-conserved
320 amino acids to recognize different sequence motifs in its target RNAs.

321 To assess the binding specificity of the Mei-P26 NHL domain experimentally, we
322 performed complementary Microscale Thermophoresis (MST) and Electrophoretic Mobility
323 Shift Assay (EMSA) experiments. MST experiments showed purified Mei-P26 NHL binds a
324 single stranded polyU RNA sequence (U₇, K_d = 1.8 ± 0.2 μM), while no interaction could be
325 detected with a folded RNA hairpin (recognized by Lin41) or a single stranded 7 nt DNA
326 oligonucleotide (TTTTACA; **Fig. 1B**). EMSA experiments confirmed the complex formation
327 between Mei-P26 NHL and a polyU RNA oligonucleotide without affecting RNA integrity
328 (**Supplementary Fig. 3C**) and verified its inability to bind other tested nucleic acids (**Fig.**
329 **1C**). The similarity between Mei-P26 NHL and Brat as well as the interaction data indicate
330 that both proteins preferentially recognize linear motifs in single-stranded RNA (ssRNA)
331 molecules.

332 **Mei-P26 NHL recognizes U-rich RNA sequences**

333 To gain further insight into the sequence specificity of Mei-P26 NHL, we used
334 recently developed algorithms (38) to re-analyze the data from RNAcompete experiments
335 previously carried out by the Hughes and Morris groups (6). We sought to obtain a complete
336 list of oligonucleotide sequences that may interact with the NHL domain of Mei-P26, as an
337 initial step of defining Mei-P26 NHL targets. In our analyses we utilized a previously
338 generated library of almost all possible 7-mer oligonucleotide fragments that have been tested
339 for binding to purified GST-tagged Mei-P26 NHL (6). The relative binding of each of the
340 sequences is presented as a Z-score calculated from a dataset computationally separated into
341 two subsets termed Set A and Set B and for a combined subsets A+B. Consensus motifs
342 recognized by Mei-P26 NHL (**Fig. 2A**) were calculated from the ten top-scored sequences of
343 7-mer motifs. Of note, we performed the same control analysis for the Brat NHL domain and
344 subsequently confirmed the binding of its RNAcompete-driven consensus motif (BRAT1:
345 UUGUAAA) using MST (**Supplementary Fig. 3A, B**). Our data are consistent with
346 previously published results (6) and show that Mei-P26 NHL preferentially binds
347 oligonucleotides including three or more consecutive uridines commonly flanked by
348 additional adenine and/or cytosine residues.

349 **Modeling of the NHL:RNA complexes**

350 To better understand the mechanistic nature of RNA binding, we performed molecular
351 dynamics (MD) simulations for the NHL domains of Mei-P26 and Brat with the U-rich RNA
352 sequences derived from RNAcompete (**Fig. 2B, Supplementary Fig. 4, Supplementary Fig.**
353 **5**). Initial models of Mei-P26 in complex with RNA (SEQ1: UUUUUUU, SEQ3:
354 UUUUACA, or BRAT1: UUGUAAA) were generated by modeling the RNA to reflect the
355 conformation of the UUGUUGU nucleotide bound to the Brat NHL domain (PDB ID: 5EX7).
356 According to our analysis, SEQ3 binds most stably to the Mei-P26 NHL domain and
357 converges into a well-defined conformation (**Fig. 2B, Supplementary Fig. 4**). Simulations

358 with the top-scored polyU oligonucleotide (SEQ1) and the inverted SEQ3 sequence
359 (ACAUUUU) resulted in much higher RMSD values, indicating a weaker fit in comparison to
360 the SEQ3 RNA (**Supplementary Fig. 4A**). The top five clusters obtained by the MD
361 simulations with SEQ3 are much more similar to each other than any of them compared to the
362 clusters obtained with SEQ1. Moreover, we observed lower variance in the 3' region and
363 more structural heterogeneity of the 5'-RNA docking site between the individual clusters of
364 the Mei-P26:UUUUACA models (**Supplementary Fig. 4B**). Together, our simulations
365 emphasize the importance of the ACA trinucleotide anchor adjacent to poly-uridine stretches
366 for Mei-P26 RNA recognition (**Fig. 2B, Supplementary Fig. 4**). Although similar affinities
367 were determined for both oligonucleotides (**Fig. 2C, Supplementary Fig. 6**), an elevated
368 value for the polyU could have been indirectly caused by the so called avidity effect (57) (**Fig.**
369 **2D**). This effect describes a scenario where an individual binding event increases the
370 probability of additional interactions occurring in its close proximity. Our *in silico* analysis,
371 together with RNAcompete results, suggests that Mei-P26 NHL may use various RNA
372 recognition modes to interact with different RNA sequences despite similar binding constants.

373 To obtain a relative comparison between models and crystal structures using the same
374 modeling restraints, we performed three control MD simulations of the Brat NHL protein with
375 both the Brat NHL and the Mei-P26 NHL top-scoring sequences from the RNAcompete
376 experiment (BRAT1: UUGUAAA, SEQ3: UUUUACA) and the co-crystallized UUGUUGU
377 nucleotide (PDB ID: 5EX7) (**Supplementary Fig. 5A**). Interestingly, the Brat NHL top-
378 scoring sequence (BRAT1) from the RNAcompete experiment showed a relatively similar
379 RMSD profile to the Mei-P26 NHL top-scoring sequence (SEQ3). Even if the model of
380 crystallized Brat: UUGUUGU complex shows the lowest RMSD in comparison to the starting
381 model, we still observed a slight structural divergence from the obtained crystal structure
382 (**Supplementary Fig. 5B**). Strikingly, the MD simulations for both Mei-P26 NHL:SEQ3 and

383 Brat NHL:BRAT1 complexes are of a similar range (**Supplementary Fig. 4, Supplementary**
384 **Fig. 5**), but to show the atomic importance of individual residues the obtained models cannot
385 substitute the crystal structures. Notably, the RMSD profile of Brat NHL:SEQ3 increases later
386 during simulations, while the Mei-P26 NHL:SEQ3 complex remains stable, indicating that the
387 ACA trinucleotide does not adapt well to the Brat NHL surface. During the simulation of the
388 Brat-BRAT1 complex, the guanosine nucleotide remains in a stable interaction with the
389 binding pocket further supporting its essential role in sequence-specific RNA recognition by
390 Brat. Hence, our computational analyses support the premise that Mei-P26 and Brat have very
391 distinct RNA recognition modes.

392 **Experimental characterization of the RNA target specificity of Mei-P26** 393 **NHL**

394 Next, we set out to experimentally validate the target predictions and performed *in*
395 *vitro* binding experiments using the six top ranked RNA sequences. Our results show that
396 untagged Mei-P26 NHL interacts with four of the identified 7-nt RNA oligonucleotides at
397 affinities that would be expected for specific but transiently associated RBPs (**Fig. 2C,**
398 **Supplementary Fig. 6**). Among the identified sequences, Mei-P26 NHL showed the highest
399 affinities towards SEQ3 (K_d 1.7 μ M) and polyU (K_d 1.8 μ M). Mei-P26 NHL also exhibited
400 measurable affinities to the SEQ2 and SEQ5 RNA oligonucleotides but binding to SEQ4 and
401 SEQ6 was reduced. Limited solubility of purified Mei-P26 NHL protein at higher
402 concentrations did not allow determination of the dissociation constants for these
403 oligonucleotides. These data demonstrate sequence-specific recognition and discrimination by
404 the Mei-P26 NHL domain.

405 To gain further insights into the RNA sequence preferences of Mei-P26 NHL, we
406 systematically altered individual positions and features of oligonucleotides identified as Mei-
407 P26 NHL ligands. First, we added uridine nucleotides at the 5' end of SEQ3, which resulted in

408 an increased binding affinity (**Fig. 2D**). This observation agrees well with the finding that
409 Mei-P26 NHL also displays an increased affinity towards extended polyU sequences (e.g. U₉;
410 **Fig. 2D**). Of note, NHL domains usually bind to relatively short RNA motifs and specifically
411 recognize only a few nucleobases. For instance, the NHL domain of Brat establishes contacts
412 with only six consecutive bases (6), while Lin41 only recognizes two nucleobases and makes
413 most of its contacts via the ribose-phosphate backbone (3). Hence, we assume that the NHL
414 domain of Mei-P26 also recognizes a short stretch of bases (**Fig. 2B, Supplementary Fig. 4**).
415 Furthermore, we created an inverted SEQ3 oligonucleotide (ACAUUUU; **Fig. 2D**), which
416 exhibited decreased affinity and indicated the necessary 5' to 3' directionality of the motif.
417 Analysis performed with a UUUUCAC sequence also displayed significantly lower affinity
418 further indicating the importance of the ACA anchor (**Fig. 2D**). We also managed to convert
419 a poor substrate (UUUACAA) into a substrate able to be bound by the addition of a single U
420 nucleotide (UUUUACAA), highlighting the necessity of at least four consecutive uridines.
421 Conversely, insertion of a guanosine nucleotide at asymmetric and symmetric positions into
422 the polyU sequence (SEQ1) reduced the affinity to Mei-P26 (**Fig. 2D**). Extending SEQ1 by
423 two additional uridines, lead to the observation of increased affinity, illustrating the
424 aforementioned avidity effect for polyU sequences (57) (**Fig. 2D**). In summary, our results
425 show sequence-specific RNA recognition by the Mei-P26 NHL domain and confirm
426 computational predictions based on the RNAcompete data.

427 **Identification of key residues involved in RNA recognition**

428 The comparison of the Mei-P26 and Brat NHL domain structures prompted us to
429 analyze the key features of these domains involved in sequence-specific RNA recognition.
430 The models of the Mei-P26 NHL domain in complex with different RNA ligands
431 (**Supplementary Fig. 4**) allowed high confidence prediction of surface areas and individual
432 amino acids important for RNA binding. We predicted Arg1017 to be in close proximity to

433 the first base (U1) that could stack with Y999 (**Fig. 3A**). Lys1172 and Arg1175 are predicted
434 to be in hydrogen bonding distance to the fourth and sixth base (U4, C6) of the RNA
435 substrate, respectively. Moreover, in our MD experiment for Mei-P26 with SEQ3, Arg1175
436 was predicted to interact with the second, third, fourth and fifth base (U2, U3, U4, A5), while
437 Arg1150 is likely to interact with A5, C6 and A7. Importantly, for Mei-P26 simulations with
438 polyU, we did not observe an interaction of K1172 and R1150 with the RNA, suggesting that
439 they might be involved in the recognition of the ACA anchor of the target RNAs. The docking
440 analyses both emphasize the importance of the positively charged surface patch for RNA
441 binding and highlight the potential contributions of three flexible loop regions that contain
442 several positively charged residues. To confirm this hypothesis, we generated variants of Mei-
443 P26 NHL carrying alanine substitutions of the individual residues (Mei-P26 NHL_{Y999A}, Mei-
444 P26 NHL_{R1017A}, Mei-P26 NHL_{K1172A} and Mei-P26 NHL_{R1175A}), combinations thereof (Mei-
445 P26 NHL_{K1172A/R1175A}, Mei-P26 NHL_{R1150A/K1172A/R1175A} (Mei-P26^{RKR})) and deletions of the
446 longest identified loop region (Mei-P26 NHL_{ΔP1169-R1175}). Finally, we also substituted core
447 residues in the center of the positively charged cavity (Mei-P26 NHL_{R1001A/K1002A/K1192A}). All
448 variants were individually expressed in insect cells, purified and subjected to thermal shift
449 assays to confirm proper folding and stability. With the exceptions of substitutions of Tyr999
450 (Mei-P26 NHL_{Y999A}) and residues in its proximity Arg1001 and Lys1002 (Mei-P26
451 NHL_{R1001A/K1002A/K1192A}), which strongly destabilized the domain or led to protein degradation
452 (**Supplementary Fig. 7A,B**), all variants showed purity and stability parameters comparable
453 to the wild type Mei-P26 NHL protein (**Fig. 3B, Supplementary Fig. 7A,B**). We tested all
454 stable Mei-P26 NHL variants in RNA interaction assays and observed severely compromised
455 or even complete loss of complex formation with SEQ3 (**Fig. 3C**). To understand whether
456 some of the variants exhibit different motif and sequence specificity, we also tested their
457 binding to a polyU oligonucleotide (U₉ and U₁₆). Most of the variants still associate with the

458 polyU oligonucleotides, albeit with reduced affinity (**Fig. 3D**). Of note, our MD simulation
459 indicated that Arg1175 participates exclusively in SEQ3 binding, but appears dispensable for
460 polyU binding. The substitution of Arg1175 indeed strongly reduces Mei-P26 NHL ability to
461 recognize the SEQ3 sequence, but shows only minor influence on its interaction with U₉. In
462 contrast, residue Arg1017 that seems to stabilize U1 in both simulations likewise strongly
463 contributes to the binding of both, SEQ3 and U₉. This data experimentally indicates that Mei-
464 P26 might employ different modes of RNA recognition for the association with different
465 RNA motifs. Furthermore, we show that simultaneous substitution of residues R1150A,
466 K1172A and R1175A fully abolishes the binding to any of the RNA sequences tested.
467 Therefore, our findings are consistent with the MD simulations and conclude that R1150 and
468 K1172 residues are responsible for anchoring the ACA trinucleotide, while R1175 stabilizes
469 the uridine tract. In summary, our results identify particular amino acid residues critical for
470 RNA recognition.

471 We also tested binding of Mei-P26 NHL to the consensus Brat recognition sequence
472 (UUGUAAA, BRAT1), which we obtained from the RNAcompete data (**Supplementary Fig.**
473 **2A**) and which we used in our MD simulations (**Supplementary Fig. 4**). While this RNA was
474 only weakly bound by Mei-P26, a single substitution from G to U (BRAT_{mut}UUUUUAA;
475 **Fig. 2D**) generated a Mei-P26-like sequence motif and allowed binding. Similarly, in our
476 experiments, Brat NHL weakly interacts with Mei-P26 SEQ3, demonstrating the specificity of
477 its NHL domain (**Supplementary Fig. 3A**). In the NHL domain of Brat, a single point
478 substitution (R875A) located in the center of the positively charged surface area impairs
479 binding to the target sequence in the 3' UTR of the *hunchback* (*hb*) mRNA (31). In Mei-P26,
480 the corresponding residue at the same position is already an alanine (Ala1046)
481 (**Supplementary Fig. 8A, 8B**). In an attempt to mimic Brat, we replaced the alanine with
482 arginine (A1046R) in the Mei-P26 NHL domain. The substitution resulted in an overall

483 destabilization of the domain and its failure to bind RNA (**Supplementary Fig. 7B,**
484 **Supplementary Fig. 8C**).

485 **Identification of Mei-P26 target mRNAs by iCLIP**

486 To identify cellular RNA targets of Mei-P26, we performed individual-nucleotide
487 resolution UV crosslinking and immunoprecipitation (iCLIP2 (53)) experiments. As
488 *Drosophila* tissues that express Mei-P26 are not readily accessible for biochemical
489 experimentation such as iCLIP, we turned to cultured *Drosophila* Schneider 2 (S2) cells as a
490 model system. S2 cells have been frequently and successfully employed to study gene
491 regulation processes that are operating in select, specialized tissues or cells (such as the
492 germline or neurons), or that occur during specific developmental stages (6, 32, 58).
493 Moreover, these cells have served to identify the mRNA targets of numerous RNA-binding
494 proteins employing CLIP or related methodology (59–61).

495 S2 cells express only low levels of mRNAs encoding Mei-P26 (62), suggesting that
496 endogenous Mei-P26 protein is not abundant. To overcome this limitation, we transfected
497 constructs encoding FLAG-tagged proteins as bait for the iCLIP experiments. We used full-
498 length Mei-P26 protein, its NHL domain, or the respective derivatives thereof that carry
499 substitutions that impair RNA binding (R1150A, K1172A and R1175A, **Supplementary Fig.**
500 **9A**). As expected, compared to the wild-type counterparts, variants with substitutions
501 immunoprecipitate strongly reduced amounts of RNA (**Supplementary Fig. 9B**).

502 Analyses of the iCLIP data from the wild-type proteins identify a local enrichment of
503 cross-link positions in 751 protein-coding genes for the full-length protein and 623 for the
504 NHL domain that do not exhibit a bias regarding their chromosomal origin (**Fig. 4A,B,**
505 **Supplementary Fig. 9C, Supplementary Data 1**). For both proteins, cross-linking mostly
506 occurs at sites located in the 3' UTRs of the target genes (**Fig. 4C, Supplementary Fig. 9C**).

507 When comparing the iCLIP datasets obtained for full-length Mei-P26 and the NHL domain,
508 only a moderate overlap is observed (22.1%, 249 loci, **Fig. 4A, Supplementary Data 2**). In
509 71.9% of the shared target genes, crosslinking is observed in comparable positions in the gene
510 body (at a distance of 50 nt or less, **Fig. 4D**). After removal of contaminating sequences (e.g.
511 mitochondrial transcripts, sno-RNA-derived reads, vector-derived sequences), the remaining
512 214 mRNA targets that are bound by the full length protein and the NHL domain were
513 analyzed for the occurrence of Mei-P26 binding motifs in a region encompassing 30 nts
514 upstream and 20 nts downstream of the crosslink positions. This revealed the presence of U-
515 rich motifs in proximity to the respective crosslink peaks in 128 mRNAs (59.8%), 65 (30%)
516 of which represent *bona fide* Mei-P26 target sequences (**Fig. 4D, 4F, Supplementary Data**
517 **2**). Hence, in proximity to the iCLIP peaks, *bona fide* Mei-P26 motifs occur at a ~9 fold
518 higher frequency than expected by chance ($f=3.4%$ expected in random 50mer RNA
519 fragments), validating the computational and experimental *in vitro* binding studies. Further
520 analyses of the mRNAs that are bound by both, full-length Mei-P26 and its NHL domain,
521 reveal an enrichment of genes encoding ribosomal proteins and translation factors (**Fig. 4E**),
522 hinting at a potential function of Mei-P26 in the control of the translation machinery which
523 was previously proposed (21). Several of the newly identified, potential RNA targets from the
524 iCLIP analyses were chosen for validation experiments employing the recombinant Mei-P26
525 NHL domain. In all cases, EMSA experiments confirmed the interaction and again the Mei-
526 P26 NHL^{RKR} mutant did not associate with the RNAs (**Fig 4F, Supplementary Fig. 10**).

527 **The NHL domain is important for Mei-P26 gene-regulatory activity**

528 To better understand the impact of Mei-P26 on gene expression, we conducted a series
529 of reporter assays in cultured *Drosophila* Schneider 2 cells. We first used the phage-derived
530 lambda-boxB system to artificially recruit full-length Mei-P26 to an RNA. For this, the
531 lambda bacteriophage antiterminator protein N (lambdaN) was fused to Mei-P26 and two

532 control proteins (Brat and GW182) to tether them to a firefly reporter RNA that contains
533 within its 3' UTR several copies of the lambdaN binding site (boxB). The same proteins
534 without the lambda peptide served as controls. In addition, a co-transfected plasmid encoding
535 a renilla luciferase mRNA that lacks the boxB elements was used for normalization. In this
536 experimental setup, Brat and the positive control GW182, which is involved in miRNA-
537 mediated gene silencing, convey robust repression of the firefly luciferase reporter mRNA
538 (31). In contrast, Mei-P26 exhibits only a weak gene regulatory activity (**Fig. 5A**).

539 Next, we analyzed expression of a reporter RNA that contains a fragment of the *nanos*
540 3'UTR, a genetically identified target of Mei-P26 (18). Co-expression of full-length Mei-P26
541 resulted in silencing of the reporter relative to a control mRNA that bears a 3' UTR from an
542 unrelated RNA (*msl-2*). Repression is dependent on the ability of Mei-P26 to bind to RNA
543 through its NHL domain since the RKR substitution abolishes regulation (**Fig. 5B**). A
544 previously identified U-rich RNA sequence element in the 3'UTR of *nanos* mRNA (29) is
545 critical for Mei-P26-mediated repression as its deletion completely abrogates regulation of the
546 reporter (**Fig. 5B**). Using a similar experimental setup, we tested a series of selected mRNA
547 targets that we identified in our iCLIP analyses (**Fig. 5C**). We included all RNA candidates
548 for which we confirmed Mei-P26 interaction and targets that contain (e.g. *Hrb27c*) or lack
549 (e.g. *spz*) the recognition motif (**Fig. 4F, Supplementary Fig. 10, Supplementary data 2**).
550 The effect of Mei-P26 on the expression of the reporters was diverse. For instance, we could
551 not detect a significant change to the expression of reporters that bear the 3'UTRs of *bic*, *chic*
552 and *RpS23*. In contrast, *LanA-*, *Mlc-c-*, *lost-* and *Hrb27C-*derived reporters exhibited
553 significant repression. Unexpectedly, *RpS20-*, *sqd-*, *sta-*, *Swip-1*, *spz-*, *eIF4A-*, *Col4A1-* and
554 *Hsp83-*derived reporters showed Mei-P26-dependent activation (**Fig. 5C**).

555 To further dissect the functional domain requirements of Mei-P26, we analyzed the
556 regulatory activity of mutant derivatives. Substitutions in the NHL domain of Mei-P26 that

557 abrogate RNA binding activity severely blunted regulation of all reporter RNAs, underlining
558 the functional importance of the domain for activity (**Fig. 5C**). Despite being expressed at a
559 comparable level (**Supplementary Fig. 11**), a construct encompassing only the NHL domain
560 was not sufficient for regulation (**Fig. 5D**), demonstrating that additional sequences outside
561 the NHL domain are required. Previously, it has been debated whether the N-terminal RING
562 domain and its ubiquitin ligase activity contribute to the gene regulatory activity of Mei-P26
563 (21). However, deletion of the N-terminal RING domain neither abolished activation of *spz*,
564 or repression of *nos* or *Hrb27c* reporters, demonstrating that ubiquitin ligase activity is
565 dispensable in this experimental setup (**Fig. 5D**).

566 **Discussion**

567 TRIM-NHL proteins are required for proper development in metazoans and their NHL
568 domains are crucial for function (25, 31, 63, 64). Despite their evolutionarily conserved
569 architecture, NHL domains exhibit clear differences in RNA binding, recognizing diverse
570 RNA sequences or RNA hairpin structures (3, 6). A structural comparison of the NHL
571 domains of Brat, Lin41, Thin/Abba and Mei-P26 reveals similarities between Brat and Mei-
572 P26 regarding their interactions with ssRNA, while Lin41 employs a different mode of
573 interaction. Although none of our numerous attempts yielded co-crystals of the Mei-P26 NHL
574 domain in complex with its RNA substrate, computational modelling allowed us to identify
575 and experimentally validate key amino acid residues involved in RNA recognition. For
576 instance, Mei-P26 and Brat employ an evolutionary conserved interaction site to specifically
577 recognize a uridine base in the first position of their RNA target. In contrast, recognition of
578 other bases differs between the two proteins and they utilize different amino acid residues for
579 substrate binding, resulting in different RNA specificity. While Brat preferentially associates
580 with a UUGUUGU RNA sequence, Mei-P26 recognizes a linear UUUUACA core motif
581 indicating at least two distinct interaction modes between these two similar NHL domains.

582 Typically, individual RNA-binding domains recognize short RNA motifs of 3-5
583 nucleotides in length with rather moderate affinities (65). To increase affinity and specificity,
584 often multiple binding domains are combined, either in tandem in the same polypeptide, or *in*
585 *trans* through formation of protein complexes (66). Our measured affinities are in the
586 micromolar range and are lower for Brat NHL than previously described for longer
587 oligonucleotide sequences (6), but comparable to those reported for CeLin41 NHL for shorter
588 hairpins (3). We provide experimental evidence (**Supplementary Fig. 9B**) that in Mei-P26
589 protein regions outside the NHL domain also contribute to RNA target recognition/binding. *In*
590 *vivo*, it is most likely that additional protein partners contribute to stable complex formation
591 between Mei-P26 and its RNA targets. Genetic experiments demonstrated that besides Mei-
592 P26, the proteins Sxl, Bam, Bgcn and Wuho are crucial for the repression of Nanos protein
593 production and differentiation of ovarian stem cells in the female germline (19, 29, 30, 67,
594 68). For regulation, these proteins likely form a large repressor complex on the 3'UTR of *nos*
595 mRNA (18, 67). Genetic ablation of any one of these proteins impaired regulation and
596 resulted in strong phenotypes (19, 30, 69–73), demonstrating that these factors need to act
597 jointly to achieve their function.

598 Moreover, we find surprising evidence that Mei-P26 not only functions in the
599 repression of selected target mRNAs but acts as an activator on other mRNAs (**Fig. 5C**). How
600 can these two seemingly different activities be explained? In tethering experiments, where the
601 closely related protein Brat acts as a strong silencer of gene expression, Mei-P26 exhibits only
602 weak activity. This suggests that either tethering disturbs its function or Mei-P26 itself is not a
603 strong regulator of gene expression. In the latter scenario, Mei-P26 might function in
604 promoting complex assembly, recruiting other factors that act in gene regulation. Previously,
605 Ago1, Sxl, Bam, Bgcn and Wuho have been identified as co-repressors that act in concert
606 with Mei-P26 in post-transcriptional regulation of gene expression (**Fig. 5E**) (18, 19, 21, 30,

607 74). Potential activators that can be recruited by Mei-P26 for gene regulation remain to be
608 identified.

609 Previously, it has been speculated that the N-terminal RING finger ubiquitin ligase
610 domain is important for Mei-P26-mediated regulation of gene expression by promoting the
611 turnover of RNA regulatory factors (21). Our data demonstrate that the Mei-P26 RING
612 domain is dispensable for regulatory activity. Similarly, the closely related protein Brat, a
613 potent post-transcriptional regulator of gene expression, has a truncated TRIM domain that
614 lacks the RING motif. However, in contrast to Brat, where the NHL domain alone was able to
615 provide most of the activity of the full-length protein (22, 23), the isolated NHL domain of
616 Mei-P26 does not exhibit gene regulation in functional assays (**Fig. 5D**).

617 iCLIP experiments allowed us to identify and validate Mei-P26 binding sites in
618 numerous transcripts. However, the S2 cells that we employed for our experimentation
619 express only a limited set of mRNAs, lacking most germline- and neuron-specific transcripts.
620 Our analysis is thus limited to the identification of Mei-P26 binding sites present in the
621 repertoire of expressed RNAs. Moreover, interacting partners likely shape the interaction
622 profile of Mei-P26 *in vivo*. In *Drosophila* this has been well documented and analyzed in
623 molecular detail for the protein Upstream of N-ras (Unr). In female flies, Unr is recruited to
624 the *msl-2* mRNA by the protein Sxl through highly synergistic interactions (75–78). We have
625 provided the first experimental evidence that the NHL domain of Mei-P26 binds to the 3'
626 UTR of *nanos* mRNA (which is not expressed in S2 cells (62)) in a mutually exclusive
627 fashion, suggesting that repressive complex formation on this transcript requires additional
628 factors such as Sxl, Bam and Bgcn. As judged by the expression level of the corresponding
629 mRNAs (Cherbas et al., Genome Res, 2011), these proteins presumably have extremely low
630 abundance in S2 cells and thus, most likely, cannot significantly impact on the RNA
631 interaction profile of Mei-P26.

632 Despite these limitations, our experimentation allowed us to identify numerous
633 transcripts that encode translation factors and ribosomal proteins among the Mei-P26 target
634 mRNAs. Previously, Mei-P26, like Brat, has been broadly implicated in the regulation of
635 ribosome biogenesis by controlling the expression of *Myc* (21, 79, 80), which stimulates the
636 expression of the Pol I transcriptional machinery thus promoting ribosome biogenesis (21, 81,
637 82). The coordinate regulation of ribosomal proteins and ribosomal RNA (rRNA) synthesis by
638 Mei-P26 might allow it to efficiently tune ribosome biosynthesis which is linked to cell
639 growth and the switch between proliferation and differentiation.

640 In summary, our computational, *in vitro* and *in vivo* studies provide a comprehensive
641 insight into RNA recognition by Mei-P26 and reveal differences to the closely related protein
642 Brat. We further identify and validate numerous novel mRNA targets of Mei-P26 and provide
643 unexpected evidence that it can function in both repression and activation of gene expression.

644 **Data availability**

645 The atomic coordinates and respective structure factors for Mei-P26 NHL (PDB ID:
646 7NYQ) have been validated and deposited at the European Protein Data Bank. Computational
647 models and description of the restraints have been deposited with Mendeley Data
648 (doi:10.17632/jvkcfwyz47.1). All sequencing data has been deposited at GEO under the
649 following accession number: GSE152013 (token for reviewers: kfwtcywofxaxlkv).

650 **Funding**

651 National Science Centre, Poland [UMO-2015/19/P/NZ1/02514 to M.G., UMO-
652 2019/32/T/NZ1/00420 to A.S.K, MAESTRO 2017/26/A/NZ1/01083 to J.M.B.]. German
653 Research Foundation [SFB960 TP B11, ME4238/1-1 to J.M., RTG2355 325443116 to O.R.];
654 German Federal Ministry of Education and Research [01ZX1401D to J.M.]; Foundation for

655 Polish Science (FNP)[TECH CORE FACILITY/2017-4/6 to S.G., TEAM/2016-3/18 to
656 J.M.B.]; IIMCB statutory funds to J.M.B.

657 **Acknowledgements**

658 We thank the staff at the beamlines 14.1 (BESSY) and P11 (PETRAIII) for support
659 during data collection and the MCB Structural Biology Core Facility (supported by the
660 TEAM TECH CORE FACILITY/2017-4/6 grant from Foundation for Polish Science) for
661 providing instruments and support. We thank Kate Nie, Debashish Ray, Timothy R. Hughes
662 and Quaid D. Morris at the University of Toronto for providing the RNAcompete data and for
663 valuable discussions on the data analysis. We thank Gunter Meister at the University of
664 Regensburg, Inga Loedige at the Max Delbrück Center for Molecular Medicine, Berlin, and
665 Julian König at the Central European Institute of Molecular Biology, Mainz, for sharing
666 reagents. We thank Panagiotis Alexiou at the Central European Institute of Technology, Brno,
667 for discussions on CLIP data analysis. We thank Elizabeth Michalczyk for useful comments
668 on the revised manuscript. This project has received funding from the European Union's
669 Horizon 2020 research and innovation programme under the Marie Skłodowska-Curie grant
670 agreement No. 665778 (M.G. and A.S.K.). Computational analyses were performed using the
671 resources of IIMCB, the Poznań Supercomputing and Networking Center at the Institute of
672 Bioorganic Chemistry, Polish Academy of Sciences (grant: 312), the Polish Grid
673 Infrastructure (grants: rnpmd, rnpmc and simcryox) and the Interdisciplinary Centre for
674 Mathematical and Computational Modelling at the University of Warsaw (grants: G73-4 and
675 GB76-30). The open-access publication of this article was funded by the BioS Priority
676 Research Area under the program "Excellence Initiative – Research University" at the
677 Jagiellonian University in Krakow

678 **Author contributions**

679 ASK performed biochemical, biophysical and crystallographic analyses; ASK cloned
680 and purified proteins and characterized variants using biophysical analyses with the help of
681 AK and MG; ASK and SG collected crystallographic data, refined structures and analyzed the
682 crystallographic results. ASK and AH analyzed RNA-protein interaction *in vitro*. AH and OR
683 performed *in vivo* analysis with the help of DS and JM. PG, CN and JMB conducted
684 computational analyses and structure modeling. JM, MG and SG envisioned the project and
685 designed the experimental concepts. ASK, JM and SG prepared figures. ASK, MG, JM and
686 SG wrote the manuscript, with the input from all other authors.

687 **Conflict of interest**

688 Janusz M. Bujnicki is Executive Editor of Nucleic Acids Research.

References

- 690 1. Corley,M., Burns,M.C. and Yeo,G.W. (2020) How RNA-Binding Proteins Interact with RNA: Molecules and
691 Mechanisms. *Mol. Cell*, **78**, 9–29.
- 692 2. Castello,A., Fischer,B., Eichelbaum,K., Horos,R., Beckmann,B.M., Strein,C., Davey,N.E., Humphreys,D.T.,
693 Preiss,T., Steinmetz,L.M., *et al.* (2012) Insights into RNA Biology from an Atlas of Mammalian mRNA-
694 Binding Proteins. *Cell*, **149**, 1393–1406.
- 695 3. Kumari,P., Aeschmann,F., Gaidatzis,D., Keusch,J.J., Ghosh,P., Neagu,A., Pachulska-Wieczorek,K.,
696 Bujnicki,J.M., Gut,H., Großhans,H., *et al.* (2018) Evolutionary plasticity of the NHL domain underlies
697 distinct solutions to RNA recognition. *Nat. Commun.*, **9**.
- 698 4. Kwon,S.C., Yi,H., Eichelbaum,K., Föhr,S., Fischer,B., You,K.T., Castello,A., Krijgsveld,J., Hentze,M.W. and
699 Kim,V.N. (2013) The RNA-binding protein repertoire of embryonic stem cells. *Nat. Struct. Mol. Biol.*, **20**,
700 1122–1130.
- 701 5. Loedige,I., Gaidatzis,D., Sack,R., Meister,G. and Filipowicz,W. (2013) The mammalian TRIM-NHL protein
702 TRIM71/LIN-41 is a repressor of mRNA function. *Nucleic Acids Res.*, **41**, 518–532.
- 703 6. Loedige,I., Jakob,L., Treiber,T., Ray,D., Stotz,M., Treiber,N., Hennig,J., Cook,K.B., Morris,Q., Hughes,T.R.,
704 *et al.* (2015) The Crystal Structure of the NHL Domain in Complex with RNA Reveals the Molecular
705 Basis of Drosophila Brain-Tumor-Mediated Gene Regulation. *Cell Rep.*, **13**, 1206–1220.
- 706 7. Borden,K.L.B. (1998) RING fingers and B-boxes: Zinc-binding protein-protein interaction domains. *Biochem.*
707 *Cell Biol.*, **76**, 351–358.
- 708 8. Reddy Bramham A., Etkin Laurence D.,F.P.S. (1992) A novel zinc finger coiled-coil domain in a family of
709 nuclear proteins.
- 710 9. Reymond,A., Meroni,G., Fantozzi,A., Merla,G., Cairo,S., Luzi,L., Riganelli,D., Zanaria,E., Messali,S.,
711 Cainarca,S., *et al.* (2001) The tripartite motif family identifies cell compartments. **20**.
- 712 10. Slack,F.J. and Ruvkun,G. (1998) A novel repeat domain that is often associated with RING finger and B-box
713 motifs. *Trends Biochem. Sci.*, **23**, 474–475.
- 714 11. Williams,F.P., Haubrich,K., Perez-Borrajerro,C. and Hennig,J. (2019) Emerging RNA-binding roles in the
715 TRIM family of ubiquitin ligases. *Biol. Chem.*, **400**, 1443–1464.
- 716 12. Jin,W., Wang,Y., Chao-Pei,L., Yang,N., Jin,M., Cong,Y., Wang,M. and Rui-Ming,X. (2016) Structural basis
717 for snRNA recognition by the double-WD40 repeat domain of Gemin5. *Genes Dev.*, **30**, 2391–2403.
- 718 13. Stirnimann,C.U., Petsalaki,E., Russell,R.B. and Muller,C.W. (2010) WD40 proteins propel cellular
719 networks. *Trends Biochem Sci*, **35**, 565–574.
- 720 14. Tocchini,C. and Ciosk,R. (2015) TRIM-NHL proteins in development and disease. *Semin. Cell Dev. Biol.*,
721 **47–48**, 52–59.
- 722 15. Chen,D., Wu,C., Zhao,S., Geng,Q., Gao,Y., Li,X., Zhang,Y. and Wang,Z. (2014) Three RNA Binding
723 Proteins Form a Complex to Promote Differentiation of Germline Stem Cell Lineage in Drosophila. *PLoS*
724 *Genet.*, **10**.
- 725 16. Insko,M.L., Bailey,A.S., Kim,J., Olivares,G.H., Wapinski,O.L., Tam,C.H. and Fuller,M.T. (2012) A self-
726 limiting switch based on translational control regulates the transition from proliferation to differentiation in
727 an adult stem cell lineage. *Cell Stem Cell*, **11**, 689–700.
- 728 17. Li,Y., Maines,J.Z., Tastan,O.Y., McKearin,D.M. and Buszczak,M. (2012) Mei-P26 regulates the
729 maintenance of ovarian germline stem cells by promoting BMP signaling. *Development*, **139**, 1547–1556.
- 730 18. Li,Y., Zhang,Q., Carreira-Rosario,A., Maines,J.Z., McKearin,D.M. and Buszczak,M. (2013) Mei-P26
731 Cooperates with Bam, Bgcn and Sxl to Promote Early Germline Development in the Drosophila Ovary.
732 *PLoS One*, **8**, 1–7.
- 733 19. Page,S.L., McKim,K.S., Deneen,B., Van Hook,T.L. and Hawley,R.S. (2000) Genetic studies of mei-P26
734 reveal a link between the processes that control germ cell proliferation in both sexes and those that control
735 meiotic exchange in Drosophila. *Genetics*, **155**, 1757–1772.
- 736 20. Slaidina,M. and Lehmann,R. (2014) Translational control in germline stem cell development. *J. Cell Biol.*,
737 **207**, 13–21.
- 738 21. Neumüller,R.A., Betschinger,J., Fischer,A., Bushati,N., Poernbacher,I., Mechtler,K., Cohen,S.M. and
739 Knoblich,J.A. (2008) Mei-P26 regulates microRNAs and cell growth in the Drosophila ovarian stem cell
740 lineage. *Nature*, **454**, 241–245.
- 741 22. Arama,E., Dickman,D., Kimchie,Z., Shearn,A. and Lev,Z. (2000) Mutations in the β -propeller domain of the
742 Drosophila brain tumor (brat) protein induce neoplasm in the larval brain. *Oncogene*, **19**, 3706–3716.
- 743 23. Sonoda,J. and Wharton,R.P. (2001) Drosophila brain tumor is a translational repressor. *Genes Dev.*, **15**, 762–
744 773.
- 745 24. Cho,P.F., Gamberi,C., Cho-Park,Y.A., Cho-Park,I.B., Lasko,P. and Sonenberg,N. (2006) Cap-Dependent

- 746 Translational Inhibition Establishes Two Opposing Morphogen Gradients in Drosophila Embryos. *Curr.*
747 *Biol.*, **16**, 2035–2041.
- 748 25. Harris,R.E., Pargett,M., Sutcliffe,C., Umulis,D. and Ashe,H.L. (2011) Brat Promotes Stem Cell
749 Differentiation via Control of a Bistable Switch that Restricts BMP Signaling. *Dev. Cell*, **20**, 72–83.
- 750 26. Lee,C.Y., Wilkinson,B.D., Siegrist,S.E., Wharton,R.P. and Doe,C.Q. (2006) Brat is a Miranda cargo protein
751 that promotes neuronal differentiation and inhibits neuroblast self-renewal. *Dev. Cell*, **10**, 441–449.
- 752 27. Muraro,N.I., Weston,A.J., Gerber,A.P., Luschnig,S., Moffat,K.G. and Baines,R.A. (2008) Pumilio Binds
753 para mRNA and Requires Nanos and Brat to Regulate Sodium Current in Drosophila Motoneurons. *J.*
754 *Neurosci.*, **28**, 2099–2109.
- 755 28. Edwards,T.A., Wilkinson,B.D., Wharton,R.P. and Aggarwal,A.K. (2003) Model of the Brain Tumor-Pumilio
756 translation repressor complex. *Genes Dev.*, **17**, 2508–2513.
- 757 29. Chau,J., Kulnane,L.S. and Salz,H.K. (2012) Sex-lethal enables germline stem cell differentiation by down-
758 regulating Nanos protein levels during Drosophila oogenesis. *Proc. Natl. Acad. Sci. U. S. A.*, **109**, 9465–
759 9470.
- 760 30. Rastegari,E., Kajal,K., Tan,B.S., Huang,F., Chen,R.H., Hsieh,T.S. and Hsu,H.J. (2020) WD40 protein Wuho
761 controls germline homeostasis via TRIM-NHL tumor suppressor Mei-p26 in Drosophila. *Dev.*, **147**.
- 762 31. Loedige,I., Stotz,M., Qamar,S., Kramer,K., Hennig,J., Schubert,T., Löffler,P., Längst,G., Merkl,R.,
763 Urlaub,H., *et al.* (2014) The NHL domain of BRAT is an RNA-binding domain that directly contacts the
764 hunchback mRNA for regulation. *Genes Dev.*, **28**, 749–764.
- 765 32. Medenbach,J., Seiler,M. and Hentze,M.W. (2011) Translational control via protein-regulated upstream open
766 reading frames. *Cell*, **145**, 902–913.
- 767 33. Kabsch,W. (2010) XDS. *Acta Crystallogr. Sect. D Biol. Crystallogr.*, **66**, 125–132.
- 768 34. McCoy,A.J., Grosse-Kunstleve,R.W., Adams,P.D., Winn,M.D., Storoni,L.C. and Read,R.J. (2007) Phaser
769 crystallographic software. *J Appl Crystallogr*, **40**, 658–674.
- 770 35. Emsley,P. and Cowtan,K. (2004) Coot: model-building tools for molecular graphics. *Acta Crystallogr D Biol*
771 *Crystallogr*, **60**, 2126–2132.
- 772 36. Afonine,P. V., Grosse-Kunstleve,R.W., Echols,N., Headd,J.J., Moriarty,N.W., Mustyakimov,M.,
773 Terwilliger,T.C., Urzhumtsev,A., Zwart,P.H. and Adams,P.D. (2012) Towards automated crystallographic
774 structure refinement with phenix.refine. *Acta Crystallogr. Sect. D Biol. Crystallogr.*, **68**, 352–367.
- 775 37. DeLano,W.L. (2002) Pymol: An open-source molecular graphics tool. *CCP4 Newsl. Protein Crystallogr.*,
776 **40**, 82–92.
- 777 38. Ray,D., Ha,K.C.H., Nie,K., Zheng,H., Hughes,T.R. and Morris,Q.D. (2018) RNAcompete methodology and
778 application to determine sequence preferences of unconventional RNA-binding proteins. *Methods*, **8260**,
779 3–15.
- 780 39. Pettersen,E.F., Goddard,T.D., Huang,C.C., Couch,G.S., Greenblatt,D.M., Meng,E.C. and Ferrin,T.E. (2004)
781 UCSF Chimera - A visualization system for exploratory research and analysis. *J. Comput. Chem.*, **25**,
782 1605–1612.
- 783 40. Salomon-Ferrer,R., Case,D.A. and Walker,R.C. (2013) An overview of the Amber biomolecular simulation
784 package. *Wiley Interdiscip. Rev. Comput. Mol. Sci.*, **3**, 198–210.
- 785 41. Jorgensen,W.L., Chandrasekhar,J., Madura,J.D., Impey,R.W. and Klein,M.L. (1983) Comparison of simple
786 potential functions for simulating liquid water. *J. Chem. Phys.*, **79**, 926–935.
- 787 42. Maier JA, Martinez C, Kasavajhala K, Wickstrom L, Hauser KE,S.C. (2017) ff14SB: Improving the
788 accuracy of protein side chain and backbone parameters from ff99SB. *Physiol. Behav.*, **176**, 139–148.
- 789 43. Banáš,P., Hollas,D., Zgarbová,M., Jurečka,P., Orozco,M., Cheatham,T.E., Šponer,J. and Otyepka,M. (2010)
790 Performance of molecular mechanics force fields for RNA simulations: Stability of UUCG and GNRA
791 hairpins. *J. Chem. Theory Comput.*, **6**, 3836–3849.
- 792 44. Zgarbová,M., Otyepka,M., Šponer,J., Mládek,A., Banáš,P., Cheatham,T.E. and Jurečka,P. (2011)
793 Refinement of the Cornell et al. Nucleic acids force field based on reference quantum chemical
794 calculations of glycosidic torsion profiles. *J. Chem. Theory Comput.*, **7**, 2886–2902.
- 795 45. Essmann,U., Perera,L., Berkowitz,M.L., Darden,T., Lee,H. and Pedersen,L.G. (1995) A smooth particle
796 mesh Ewald method. *J. Chem. Phys.*, **103**, 8577–8593.
- 797 46. Salomon-Ferrer,R., Götz,A.W., Poole,D., Le Grand,S. and Walker,R.C. (2013) Routine microsecond
798 molecular dynamics simulations with AMBER on GPUs. 2. Explicit solvent particle mesh ewald. *J. Chem.*
799 *Theory Comput.*, **9**, 3878–3888.
- 800 47. Götz,A.W., Williamson,M.J., Xu,D., Poole,D., Le Grand,S. and Walker,R.C. (2012) Routine microsecond
801 molecular dynamics simulations with AMBER on GPUs. 1. generalized born. *J. Chem. Theory Comput.*, **8**,
802 1542–1555.
- 803 48. Le Grand,S., Götz,A.W. and Walker,R.C. (2013) SPFP: Speed without compromise - A mixed precision
804 model for GPU accelerated molecular dynamics simulations. *Comput. Phys. Commun.*, **184**, 374–380.
- 805 49. Kelley,L.A., Gardner,S.P. and Sutcliffe,M.J. (1996) An automated approach for clustering an ensemble of

- 806 NMR-derived protein structures into conformationally related subfamilies. *Protein Eng.*, **9**, 1063–1065.
- 807 50. Morris,J.H., Huang,C.C., Babbitt,P.C. and Ferrin,T.E. (2007) StructureViz: Linking Cytoscape and UCSF
- 808 Chimera. *Bioinformatics*, **23**, 2345–2347.
- 809 51. Shannon,P., Markiel,A., Ozier,O., Baliga,N.S., Wang,J.T., Ramage,D., Amin,N., Schwikowski,B. and
- 810 Ideker,T. (2003) Cytoscape: A software Environment for integrated models of biomolecular interaction
- 811 networks. *Genome Res.*, **13**, 2498–2504.
- 812 52. Theobald,D.L. and Steindel,P.A. (2012) Optimal simultaneous superpositioning of multiple structures with
- 813 missing data. *Bioinformatics*, **28**, 1972–1979.
- 814 53. Buchbender,A., Mutter,H., Sutandy,F.X.R., Körtel,N., Hänel,H., Busch,A., Ebersberger,S. and König,J.
- 815 (2019) Improved library preparation with the new iCLIP2 protocol. *Methods*, **178**, 33–48.
- 816 54. Curk,T. et al. (2019) iCount: protein-RNA interaction iCLIP data analysis. *Prep*.
- 817 55. Bawa,S., Gameros,S., Baumann,K., Brooks,D.S., Kollhoff,J.A., Zolkiewski,M., David Re Cecconi,A.,
- 818 Panini,N., Russo,M., Piccirillo,R., et al. (2020) Costameric Integrin and Sarcoglycan protein levels are
- 819 altered in a Drosophila model for Limb Girdle Muscular Dystrophy type 2H . *Mol. Biol. Cell*,
- 820 10.1091/mbc.e20-07-0453.
- 821 56. Bawa,S., Brooks,D.S., Neville,K.E., Tipping,M., Sagar,M.A., Kollhoff,J.A., Chawla,G., Geisbrecht,B. V.,
- 822 Tennessen,J.M., Eliceiri,K.W., et al. (2020) Drosophila TRIM32 cooperates with glycolytic enzymes to
- 823 promote cell growth. *Elife*, **9**, 1–29.
- 824 57. Helder,S., Blythe,A.J., Bond,C.S. and Mackay,J.P. (2016) Determinants of affinity and specificity in RNA-
- 825 binding proteins. *Curr. Opin. Struct. Biol.*, **38**, 83–91.
- 826 58. Weidmann,C.A., Qiu,C., Arvola,R.M., Lou,T.F., Killingsworth,J., Campbell,Z.T., Tanaka Hall,T.M. and
- 827 Goldstrohm,A.C. (2016) Drosophila nanos acts as a molecular clamp that modulates the RNA-binding and
- 828 repression activities of pumilio. *Elife*, **5**.
- 829 59. Moschall,R., Rass,M., Roszbach,O., Lehmann,G., Kullmann,L., Eichner,N., Strauss,D., Meister,G.,
- 830 Schneuwly,S., Krahn,M.P., et al. (2019) Drosophila Sister-of-Sex-lethal reinforces a male-specific gene
- 831 expression pattern by controlling Sex-lethal alternative splicing. *Nucleic Acids Res.*, **47**, 2276–2288.
- 832 60. Stepien,B.K., Oppitz,C., Gerlach,D., Dag,U., Novatchkova,M., Krüttner,S., Stark,A. and Keleman,K. (2016)
- 833 RNA-binding profiles of Drosophila CPEB proteins Orb and Orb2. *Proc. Natl. Acad. Sci. U. S. A.*, **113**,
- 834 E7030–E7038.
- 835 61. Hansen,H.T., Rasmussen,S.H., Adolph,S.K., Plass,M., Krogh,A., Sanford,J., Nielsen,F.C. and Christiansen,J.
- 836 (2015) Drosophila Imp iCLIP identifies an RNA assemblage coordinating F-actin formation. *Genome*
- 837 *Biol.*, **16**.
- 838 62. Cherbas,L., Willingham,A., Zhang,D., Yang,L., Zou,Y., Eads,B.D., Carlson,J.W., Landolin,J.M.,
- 839 Kapranov,P., Dumais,J., et al. (2011) The transcriptional diversity of 25 Drosophila cell lines. *Genome*
- 840 *Res.*, **21**, 301–314.
- 841 63. Nicklas,S., Otto,A., Wu,X., Miller,P., Stelzer,S., Wen,Y., Kuang,S., Wrogemann,K., Patel,K., Ding,H., et al.
- 842 (2012) TRIM32 regulates skeletal muscle stem cell differentiation and is necessary for normal adult
- 843 muscle regeneration. *PLoS One*, **7**.
- 844 64. Schwamborn,J.C., Berezikov,E. and Knoblich,J.A. (2009) The TRIM-NHL Protein TRIM32 Activates
- 845 MicroRNAs and Prevents Self-Renewal in Mouse Neural Progenitors. *Cell*, **136**, 913–925.
- 846 65. Maris,C., Dominguez,C. and Allain,F.H.T. (2005) The RNA recognition motif, a plastic RNA-binding
- 847 platform to regulate post-transcriptional gene expression. *FEBS J.*, **272**, 2118–2131.
- 848 66. Hennig,J. and Sattler,M. (2015) Deciphering the protein-RNA recognition code: Combining large-scale
- 849 quantitative methods with structural biology. *BioEssays*, **37**, 899–908.
- 850 67. Li,Y., Park,J.K., Minor,N.T., Maines,J.Z. and McKearin,D.M. (2009) Bam and Bgcn antagonize Nanos-
- 851 dependent germ-line stem cell maintenance. *Proc. Natl. Acad. Sci.*, **106**, 9304–9309.
- 852 68. Chau,J., Kulnane,L.S. and Salz,H.K. (2009) Sex-lethal facilitates the transition from germline stem cell to
- 853 committed daughter cell in the Drosophila ovary. *Genetics*, **182**, 121–132.
- 854 69. Schupbach,T. (1985) Normal Female Germ Cell Differentiation Autosome Ratio and Expression O F Sex-
- 855 Lethal. *Construction*.
- 856 70. Hashiyama,K., Hayashi,Y. and Kobayashi,S. (2011) Drosophila Sex Lethal Gene Initiates Female
- 857 Development in Germline Progenitors. *Science (80-)*, **885**, 885–888.
- 858 71. Salz,H.K., Cline,T.W. and Schedl,P. (1987) Functional changes associated with structural alterations induced
- 859 by mobilization of a P element inserted in the Sex-lethal gene of Drosophila. *Genetics*, **117**, 221–231.
- 860 72. Ohlstein,B. and McKearin,D. (1997) Ectopic expression of the Drosophila Bam protein eliminates oogenic
- 861 germline stem cells. *Development*, **124**, 3651–3662.
- 862 73. Gönczy,P., Matunis,E. and DiNardo,S. (1997) bag-of-marbles and benign genial cell neoplasm act in the
- 863 germline to restrict proliferation during Drosophila spermatogenesis. *Development*, **124**, 4361–4371.
- 864 74. Fu,Z., Geng,C., Wang,H., Yang,Z., Weng,C., Li,H., Deng,L., Liu,L., Liu,N., Ni,J., et al. (2015) Twin
- 865 Promotes the Maintenance and Differentiation of Germline Stem Cell Lineage through Modulation of

- 866 Multiple Pathways. *Cell Rep.*, **13**, 1366–1379.
- 867 75. Grskovic,M., Hentze,M.W. and Gebauer,F. (2003) A co-repressor assembly nucleated by Sex-lethal in the
868 3'UTR mediates translational control of Drosophila msl-2 mRNA. *EMBO J.*, **22**, 5571–5581.
- 869 76. Abaza,I., Coll,O., Patalano,S. and Gebauer,F. (2006) Drosophila UNR is required for translational repression
870 of male-specific lethal 2 mRNA during regulation of X-chromosome dosage compensation. *Genes Dev.*,
871 **20**, 380–389.
- 872 77. Duncan,K., Grskovic,M., Strein,C., Beckmann,K., Niggeweg,R., Abaza,I., Gebauer,F., Wilm,M. and
873 Hentze,M.W. (2006) Sex-lethal imparts a sex-specific function to UNR by recruiting it to the msl-2 mRNA
874 3' UTR: Translational repression for dosage compensation. *Genes Dev.*, **20**, 368–379.
- 875 78. Hennig,J., Militti,C., Popowicz,G.M., Wang,I., Sonntag,M., Geerlof,A., Gabel,F., Gebauer,F. and Sattler,M.
876 (2014) Structural basis for the assembly of the Sxl–Unr translation regulatory complex. *Nature*, **515**, 287–
877 290.
- 878 79. Betschinger,J., Mechtler,K. and Knoblich,J.A. (2006) Asymmetric Segregation of the Tumor Suppressor Brat
879 Regulates Self-Renewal in Drosophila Neural Stem Cells. *Cell*, **124**, 1241–1253.
- 880 80. Ferreira,A., Boulan,L., Perez,L. and Milán,M. (2014) Mei-P26 mediates tissue-specific responses to the brat
881 tumor suppressor and the dMyc Proto-Oncogene in Drosophila. *Genetics*, **198**, 249–258.
- 882 81. Frank,D.J., Edgar,B.A. and Roth,M.B. (2002) The Drosophila melanogaster gene brain tumor negatively
883 regulates cell growth and ribosomal RNA synthesis. *Development*, **129**, 399–407.
- 884 82. Grewal,S.S., Li,L., Orian,A., Eisenman,R.N. and Edgar,B.A. (2005) Myc-dependent regulation of ribosomal
885 RNA synthesis during Drosophila development. *Nat. Cell Biol.*, **7**, 295–302.
- 886

887 **Figure 1. Structure of the Mei-P26 NHL domain and its specific ssRNA**
888 **recognition**

889 **A.** Mei-P26 domain organization with NHL domain shown in blue (top left). Abbreviations:
890 RING domain (R), B-Boxes (B), coiled coil (CC), glutamine rich region (Q). Size exclusion
891 chromatography profile and SDS PAGE gel for Mei-P26 NHL protein with mass markers
892 indicated at the top. Blue line on the chromatogram corresponds to 280nm wavelength, orange
893 line to 254 nm wavelength (top right). Cartoon and surface representation of the crystal
894 structure of the Mei-P26 NHL domain in top surface and side orientations (encompassing
895 amino acids 931-1203) (left bottom). **B.** MST results for the fraction of bound DNA, dsRNA,
896 or ssRNA (U₇) ligands for different concentrations of Mei-P26 NHL. The dissociation
897 constant (K_d) was calculated from at least three independent experiments (n≥3). **C.** EMSAs
898 employing various concentrations of the Mei-P26 NHL domain (as indicated above each lane)
899 on a single-stranded DNA oligonucleotide, an RNA hairpin structure (both as indicated in the
900 MST panel), or a single-stranded U₉ RNA oligonucleotide. Depicted is a representative gel of
901 three independent replicates.

902

903 **Figure 2. The Mei-P26 NHL domain specifically recognizes single-stranded,**
904 **U-rich RNA motifs**

905 **A.** Analysis of the Mei-P26 NHL RNAcompete data. Scatter plot representing Z-scores for
906 two halves of the RNA pool (set A and set B) shown at the bottom; six highest scoring 7-mers
907 were highlighted in color in right corner of the plot. The consensus motif derived from the
908 indicated sequence motifs is indicated at the top. **B.** Comparison between the Mei-P26 NHL
909 in complex with UUUUACA (left) and UUUUUUU (right) (color-coded RNA sequences
910 depicted at the top). The complexes were computationally modelled using molecular
911 dynamics simulations by introducing oligonucleotides onto the surface of the Mei-P26 NHL
912 domain. **C, D:** MST binding studies of the NHL domain to the 6 highest scoring 7-mer
913 sequences (C), variants thereof, or the motif recognized by the closely related protein Brat
914 (D). K_d values at least three independent experiments (n≥3). MST binding curves for protein-
915 oligonucleotide complexes with calculated K_d were marked in solid lines, curves with K_d > 3
916 μM were presented as experimental points.

917

918 **Figure 3. Identification of amino acids in the NHL domain important for**
919 **RNA binding**

920 **A.** Model of the Mei-P26 NHL domain in complex with a UUUUACA RNA sequence. Select
921 amino acids predicted to be in close proximity to the RNA are highlighted. **B.** Size exclusion
922 chromatography profile and SDS-PAGE gel for selected Mei-P26 mutated variants.
923 Abbreviations for K1172A/R1175A (KR) and R1150A/K1172A/R1175A (RKR) are used in
924 the inset. **C** and **D.** MST- (panels C and D (left)) or EMSA-based (panel D (right)) *in vitro*
925 binding analyses of the recombinant NHL domain or variants thereof (as indicated in each
926 graph) to RNA oligonucleotides with the sequence UUUUACA (C), U₉ (D (left)), or U₁₆ (D
927 (right)). Dissociation constants (K_d) were calculated from three independent experiments
928 (n=3).

929

930 **Figure 4. Identification of Mei-P26 target RNAs in cultured cells**

931 **A.** Comparison of iCLIP data derived from either full-length Mei-P26 protein (depicted in
932 blue) or its NHL domain (depicted in salmon). Number of genes containing a statistically
933 significant local enrichment of cross-link positions (cross-link peaks) and percent values are
934 given for each fraction. **B.** Chromosomal origin of the 249 shared target genes identified in
935 both iCLIP datasets. **C.** Location of the full-length Mei-P26 (left) or its NHL domain-derived
936 (right) iCLIP clusters within transcripts. **D.** Presence of potential Mei-P26 RNA motifs in
937 vicinity of the cross-link peaks in the shared target genes. No overlap: cross-linking of the
938 full-length protein and the NHL domain occurred in different regions of the gene locus. **E.**
939 Gene Ontology (GO)-term analysis of biological processes enriched in the shared target
940 genes. **F.** Validation of select Mei-P26 binding sites identified by iCLIP. Top left: schematic
941 depiction of the *Hrb27c* and *Col4a1* gene loci. Introns are depicted as lines, exons as boxes;
942 the grey shading indicates the protein coding region. Below: iCLIP read depth analyses of 3'
943 UTR regions (as indicated by the solid black lines) from experiments performed with either
944 the full-length Mei-P26 protein (light blue), its NHL domain (dark blue), or from control
945 experiments (grey). Potential RNA motifs recognized by Mei-P26 are highlighted in yellow.
946 Right: EMSA analyses using RNA fragments derived from the iCLIP clusters (as indicated by
947 the red arrows, sequences provided at the bottom of the gels), using different concentrations
948 of the recombinant Mei-P26 NHL domain or its mutant derivative (Mei-P26^{RKR}: R1150A,
949 K1172A, R1175A, as indicated above the gels). Free RNA probe and NHL:RNA complexes
950 are indicated on the left.

951

952 **Figure 5. Mei-P26 regulates gene expression via 3' UTR binding sites**

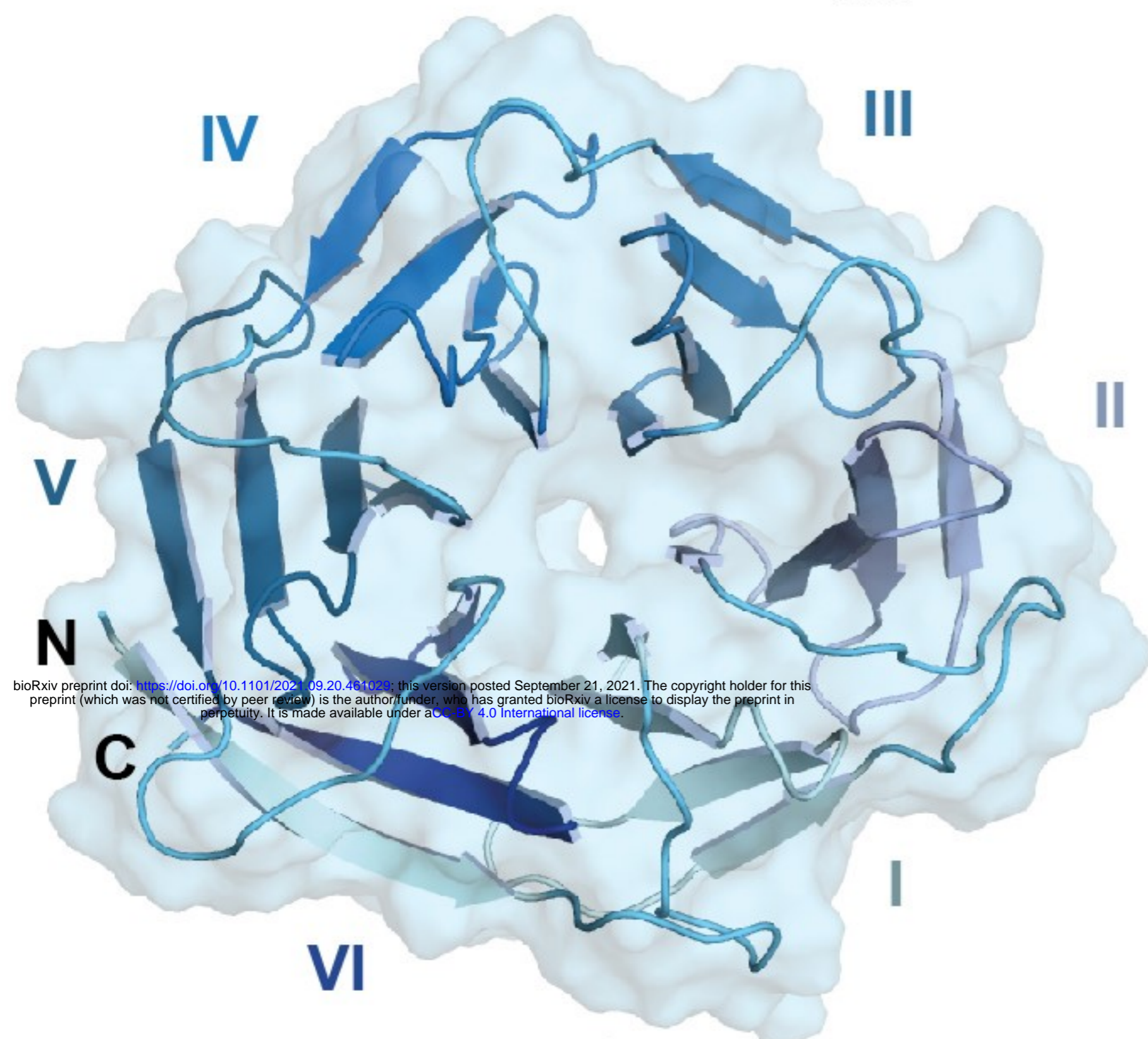
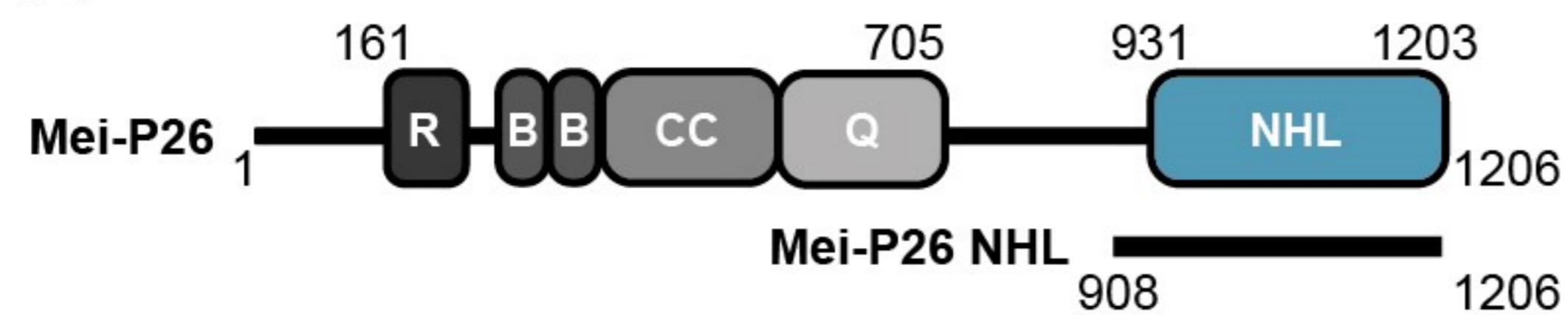
953 **A.** Tethered function assay using Brat, Gw182 (positive control) and full-length Mei-P26.
954 Activities are calculated relative to proteins that lack the tag for tethering. **B.** Mei-P26-
955 mediated repression of a reporter that either bears the *nanos* mRNA 3' UTR (*nos* wt) or a
956 version thereof in which a U-rich sequence element previously implicated in regulation was
957 mutated (*nos* mut). Reporter activity was determined in the presence of co-expressed wild-
958 type Mei-P26 protein (grey bars), or a Mei-P26 protein carrying substitutions that affect RNA
959 interaction. (Mei-P26^{RKR}:R1150A, K1172A, R1175A; black bars). All activities are
960 expressed relative to control reactions without overexpression of Mei-P26 (using an empty
961 plasmid). **C.** Reporter assays using 3' UTR sequences derived from various Mei-P26-bound
962 genes (as indicated at the bottom) and employing wt Mei-P26-FL protein (grey bars) or its
963 mutant derivative (black bars) as described for panel B. All activities are expressed relative to
964 control reactions without overexpression of Mei-P26 (using an empty plasmid). **D.** Reporter
965 assays using 3' UTR sequences of *nos* (grey), *Hrb27c* (blue) and *spz* (dark blue) derived from
966 Mei-P26-FL protein or its mutant derivatives (as indicated at the bottom) as described for
967 panels B and C. For panels a-d mean values \pm SD are depicted of at least three independent
968 biological experiments performed in three technical replicates each. P-values were calculated
969 with a two-sided student's t-test relative to the control reactions described for each panel; n.s.
970 not significant, * P-value <0.05, **: P-value <0.01, *** P-value <0.001. **E.** Schematic
971 depiction of Mei-P26-mediated post-transcriptional regulation of gene expression. Mei-P26
972 (NTD in grey, NHL domain in blue, mutated residues that are crucial for RNA binding are
973 highlighted) associates with U-rich RNA motifs present in the 3' UTRs of its RNA targets
974 (depicted schematically) to regulate their expression. Regulation involves additional factors
975 such as Ago1, Sxl, Bam, BgcN, and Wuho that have been implicated in Mei-P26-dependent
976 repression, while potential co-factors involved in Mei-P26-dependent gene activation remain
977 to be identified.

978 **Table 1: Data collection and refinement statistics**

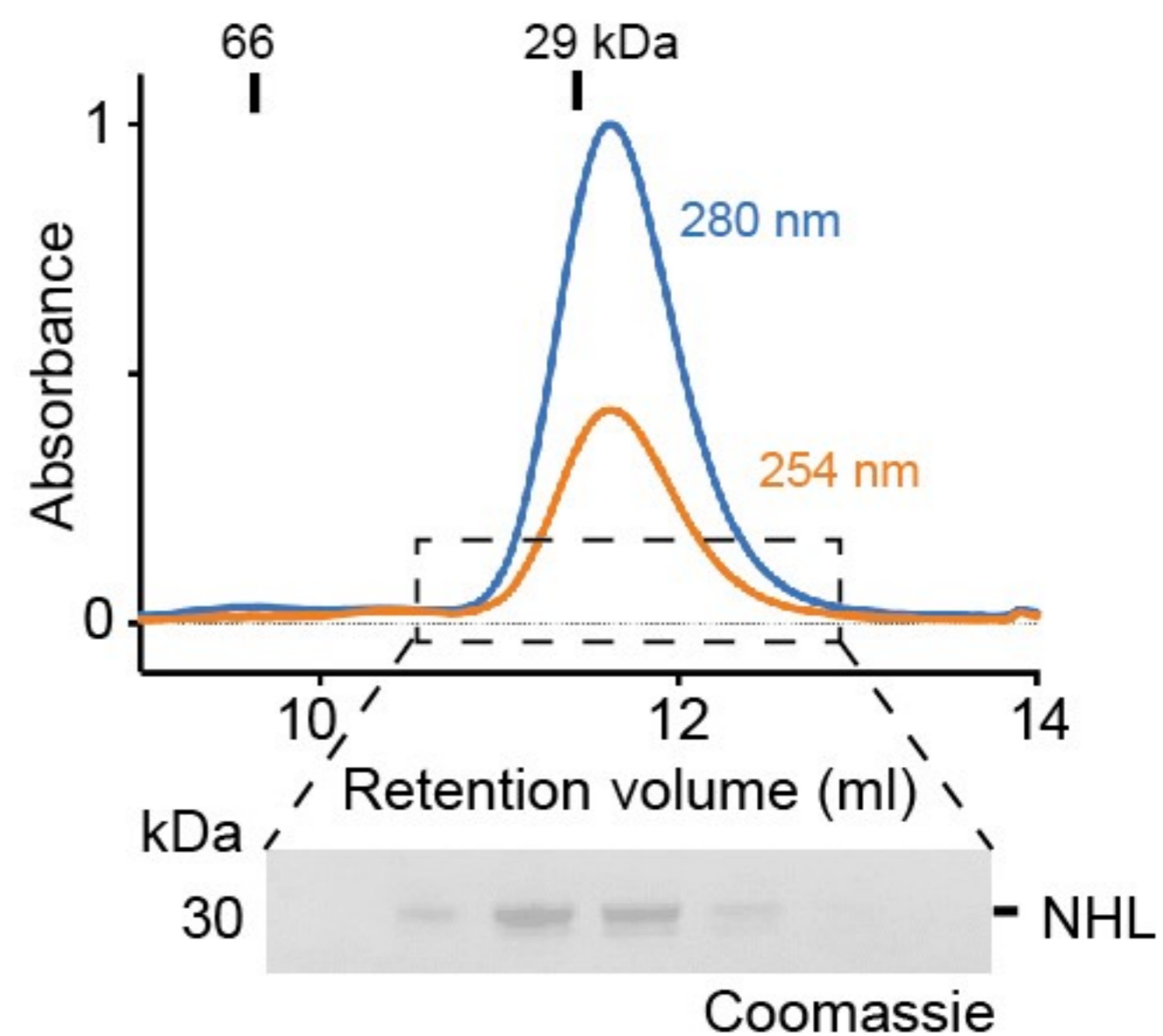
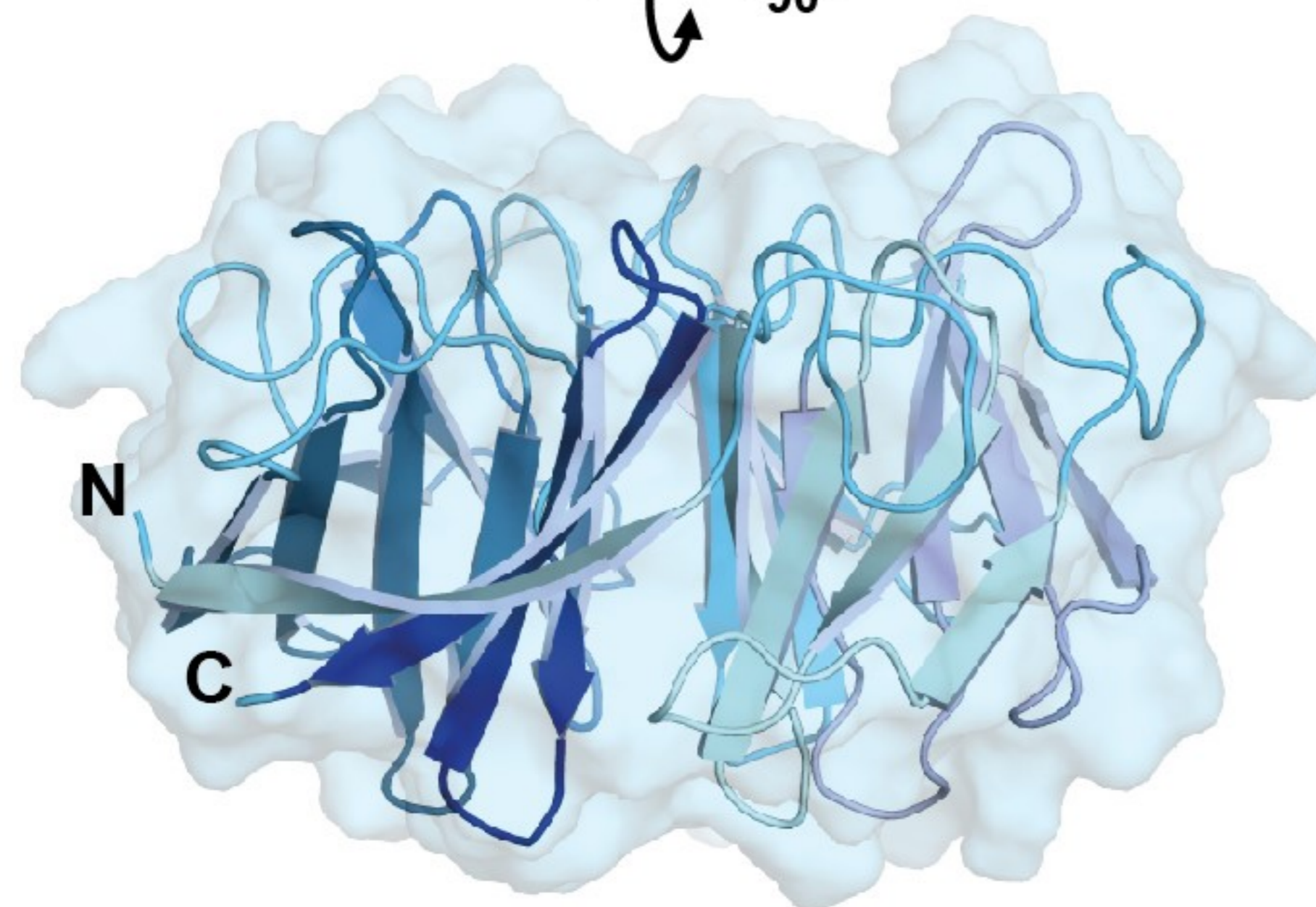
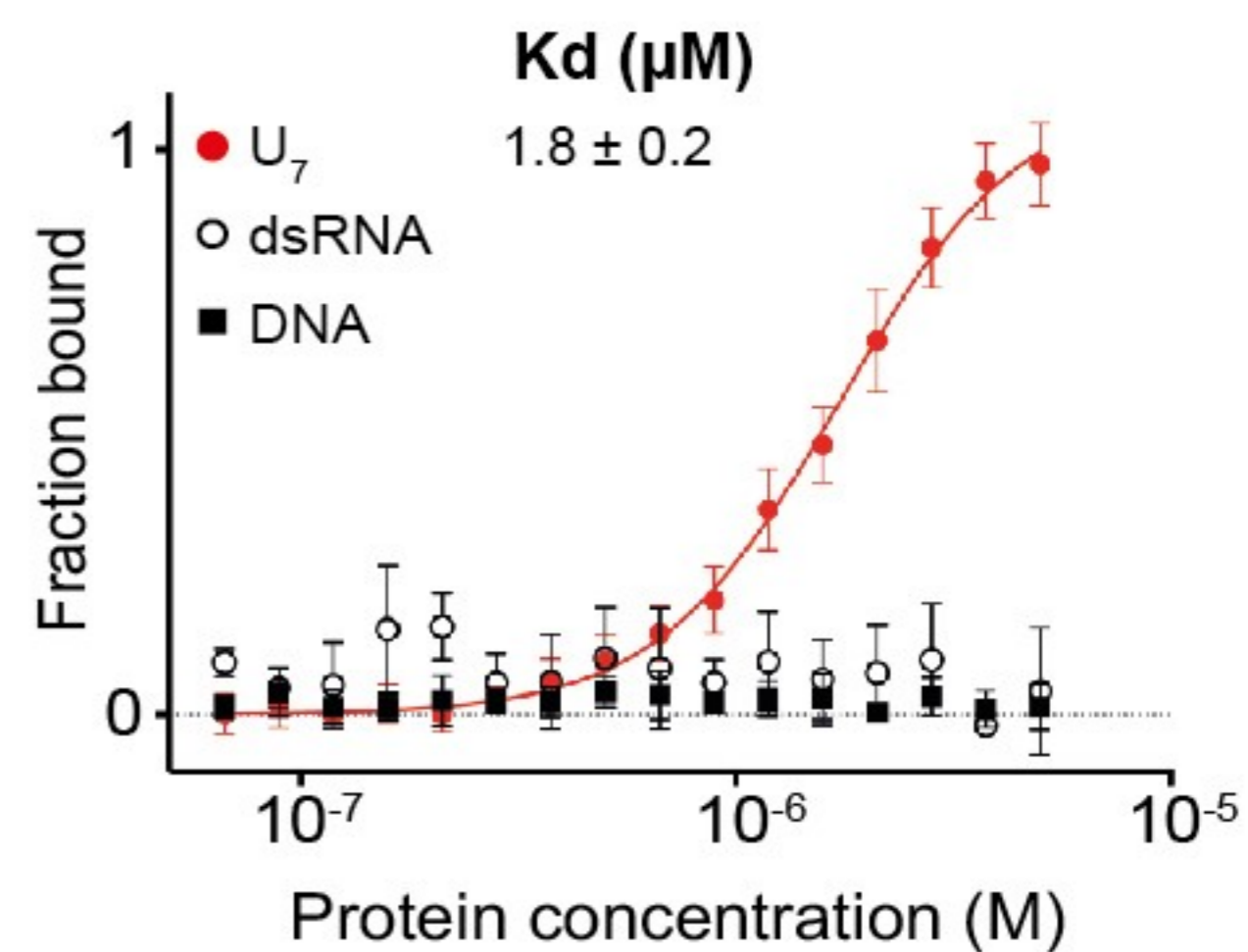
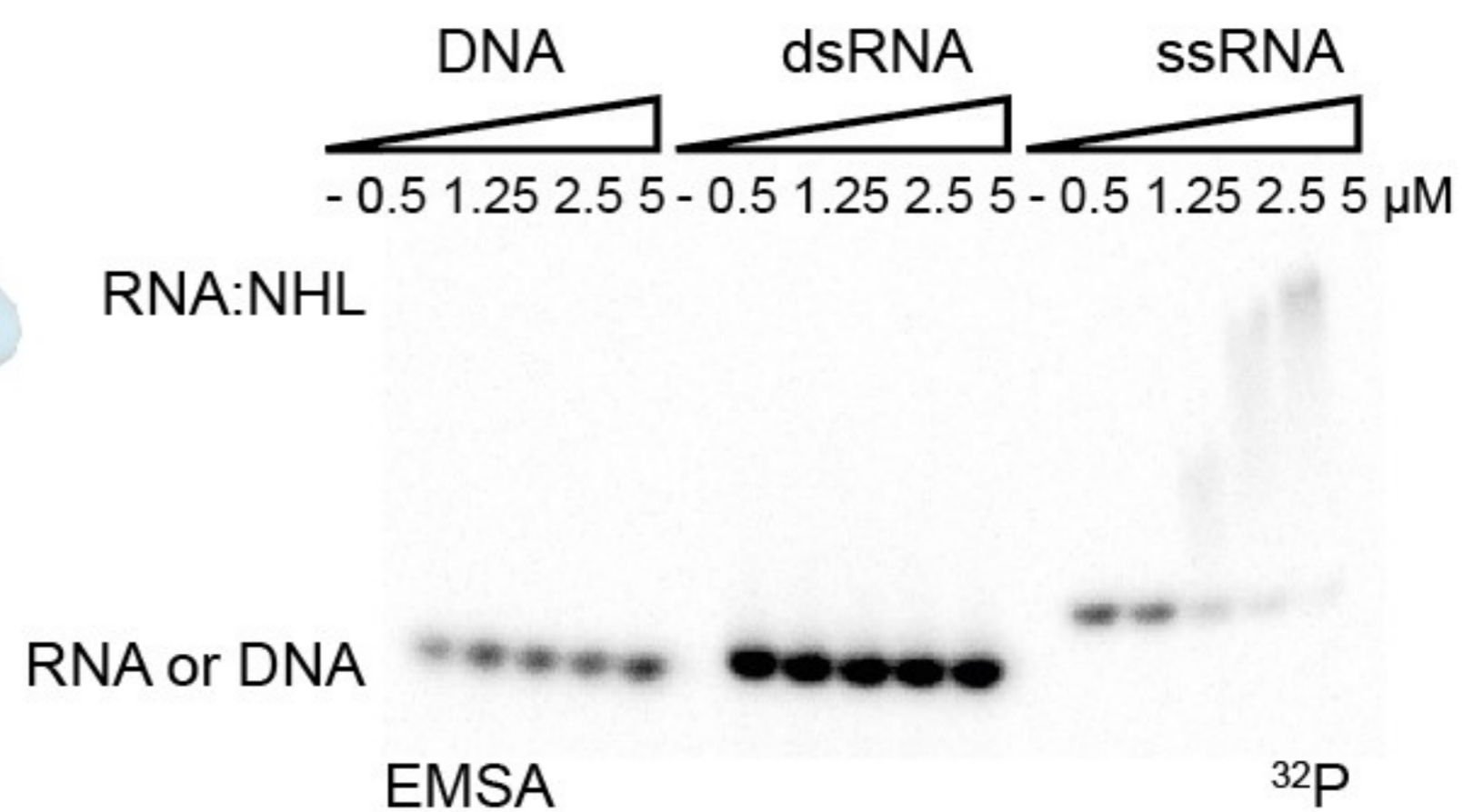
		Mei-P26 NHL PDB ID 7NYQ BESSY II, MX14-1
Data collection		
Space group		P2 ₁
Cell dimensions		
<i>a</i> , <i>b</i> , <i>c</i> (Å)		34.71 116.50 64.70
α , β , γ (°)		90 96.362 90
Wavelength		0.9184
Resolution (Å) [†]		43.17-1.6 (1.64-1.6)
<i>R</i> _{meas} (%)		7.7 (160.9)
<i>I</i> / σ (<i>I</i>)		10.15 (0.85)
<i>CC</i> _{1/2}		0.99 (0.46)
Completeness (%)		98.8 (97.0)
Redundancy		3.82
Refinement		
Resolution (Å)		43.17-1.6
No. reflections		66477
<i>R</i> _{work} / <i>R</i> _{free}		0.196 / 0.215
No. atoms		
Protein		8923
Ligand/ion		no ligands
Water		320
<i>B</i> factors		
Protein		36.7
Ligand/ion		not applicable
Water		38.3
r.m.s deviations		
Bond lengths (Å)		0.007
Bond angles (°)		0.689
Ramachandran statistics (%)	outliers	0
	allowed regions	4.59
	avored regions	95.41
Rotamer outliers (%)		0.21
Clash score		3.02
MolProbity score		1.41

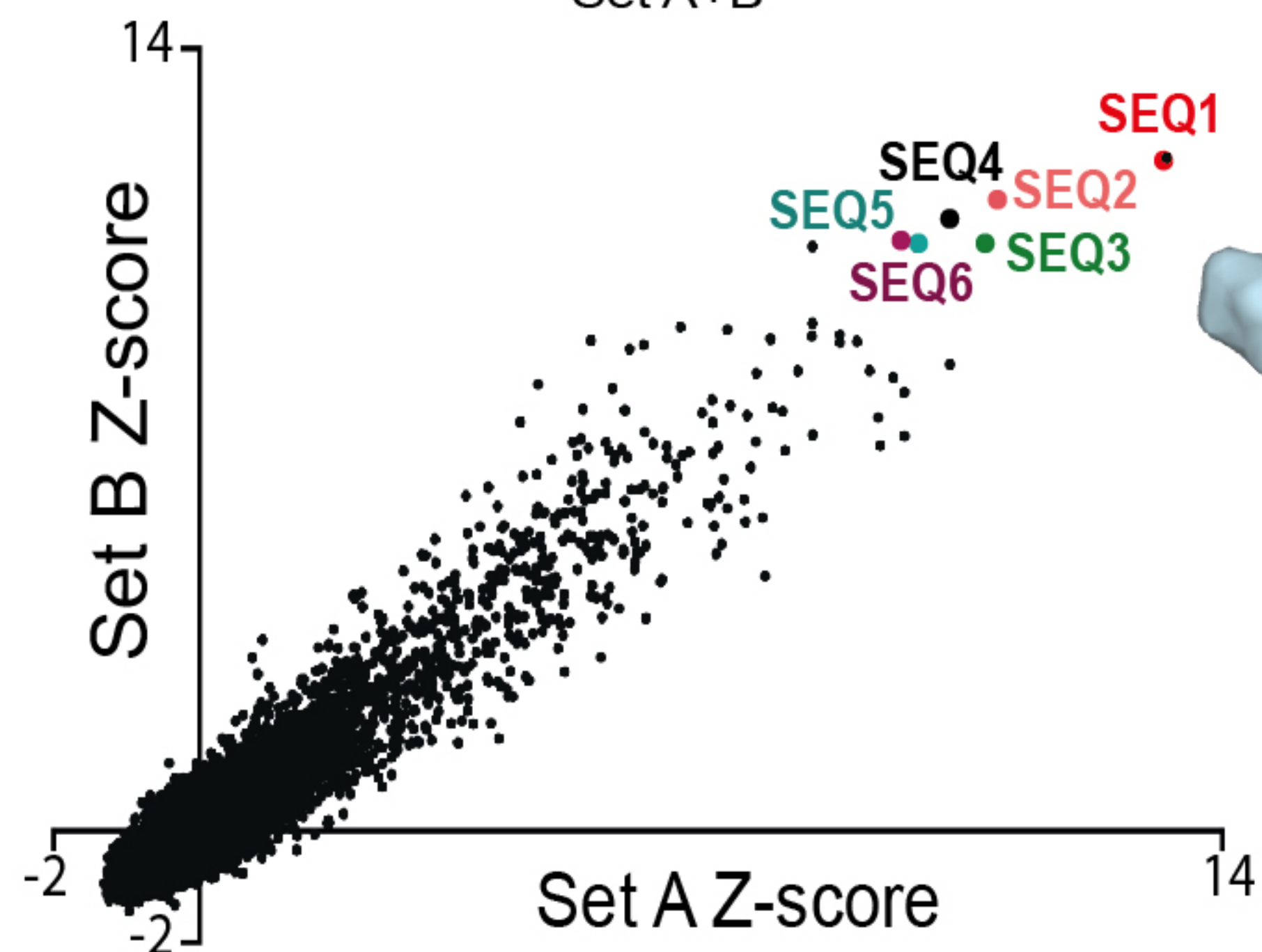
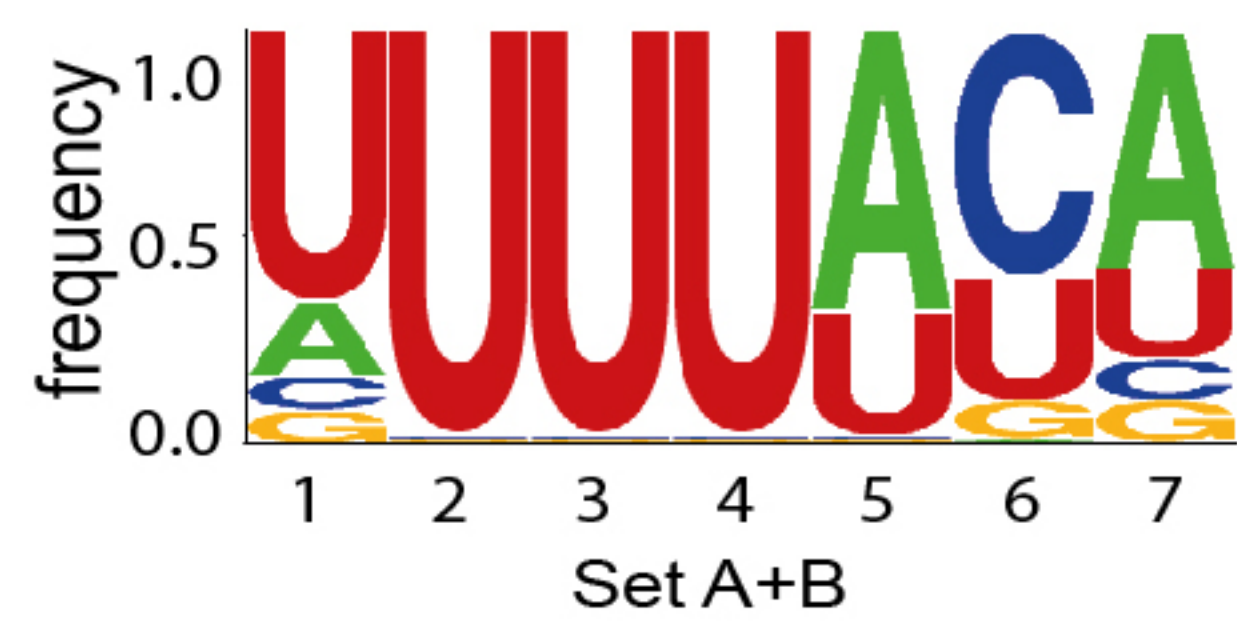
979 ^a Values in parentheses are for highest-resolution shell.

980 [†] Resolution limits according to *I*/ σ of 2 is 1.75 Å

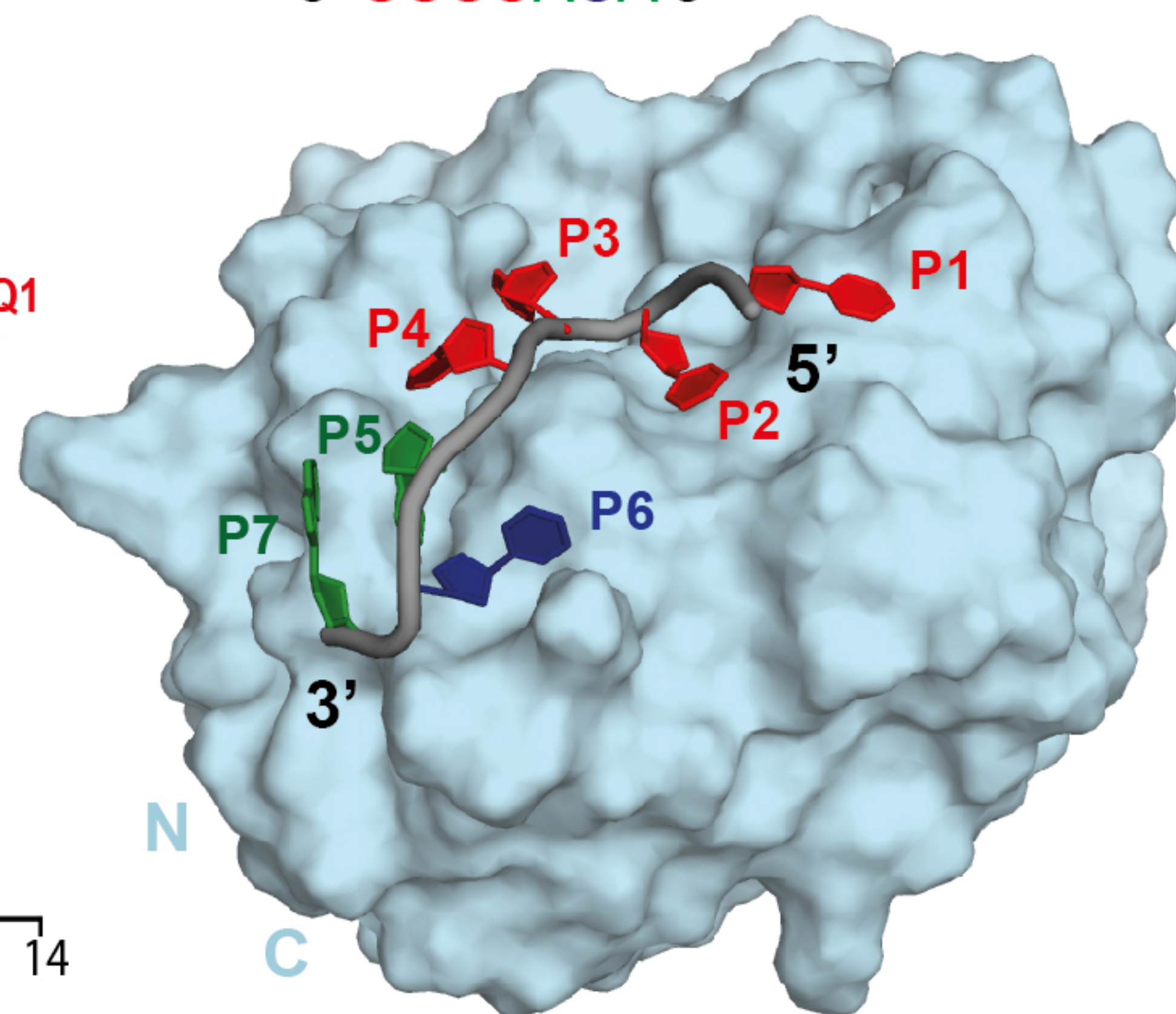
A

bioRxiv preprint doi: <https://doi.org/10.1101/2021.09.20.461020>; this version posted September 21, 2021. The copyright holder for this preprint (which was not certified by peer review) is the author/funder, who has granted bioRxiv a license to display the preprint in perpetuity. It is made available under aCC-BY 4.0 International license.

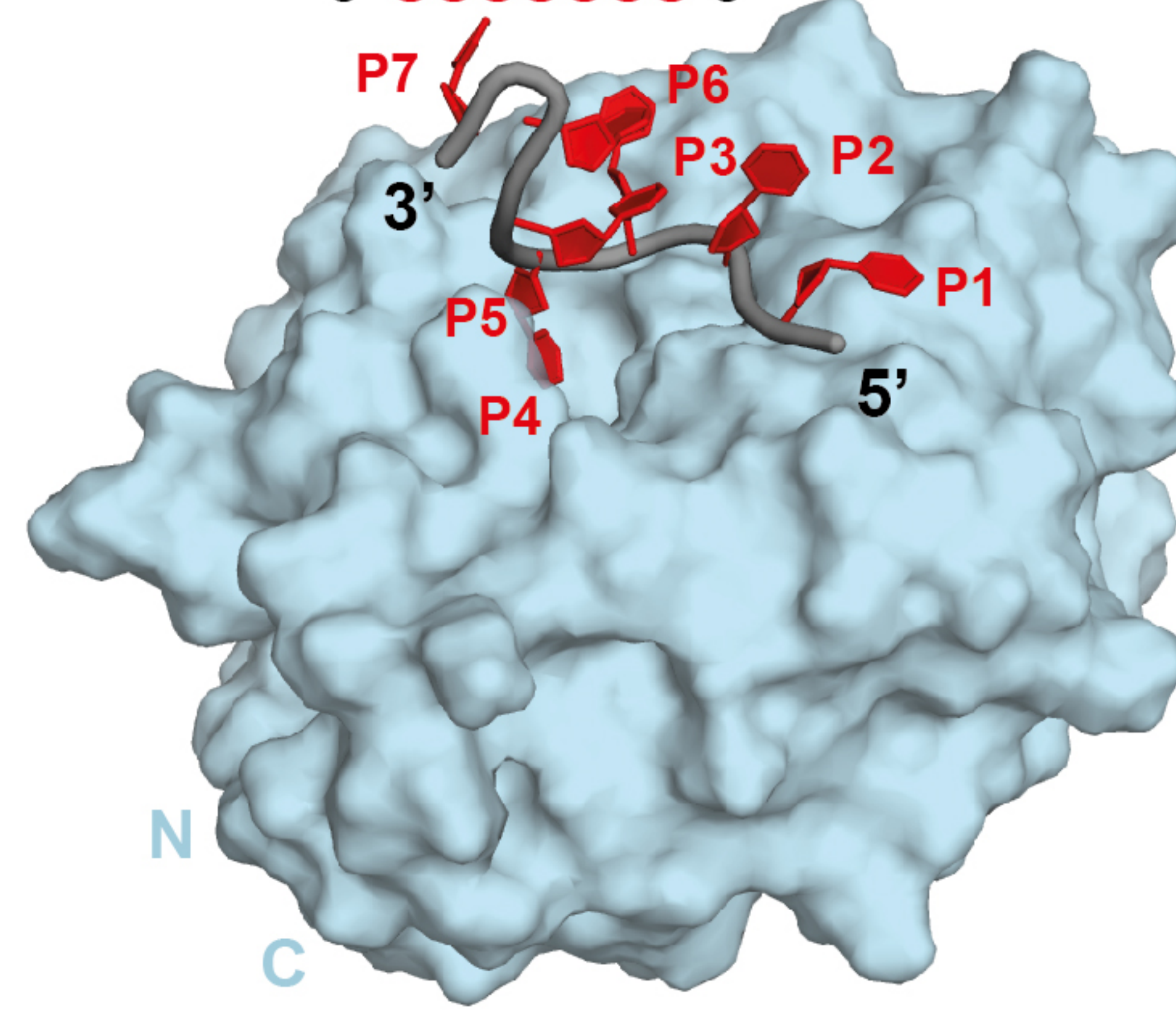
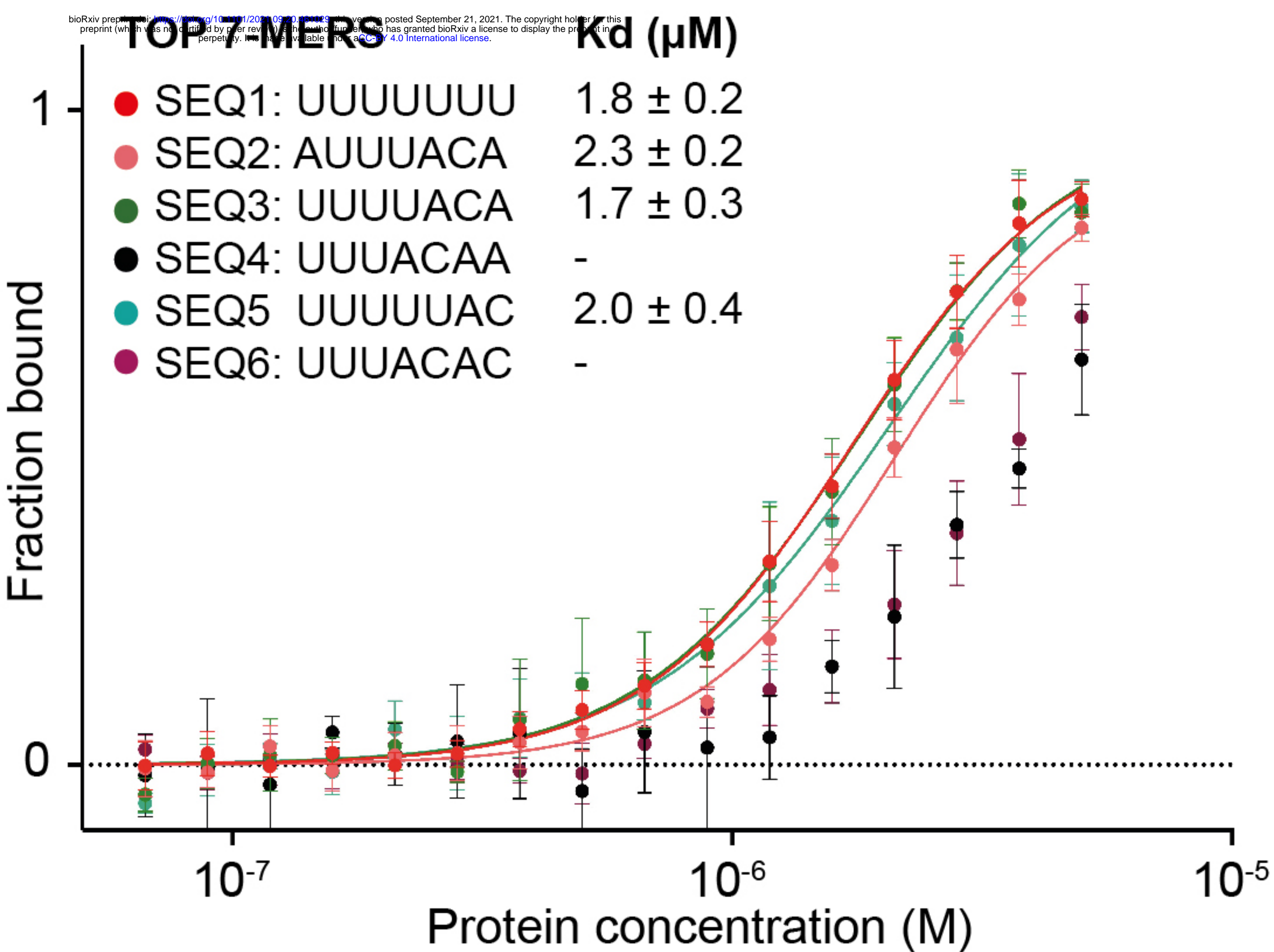
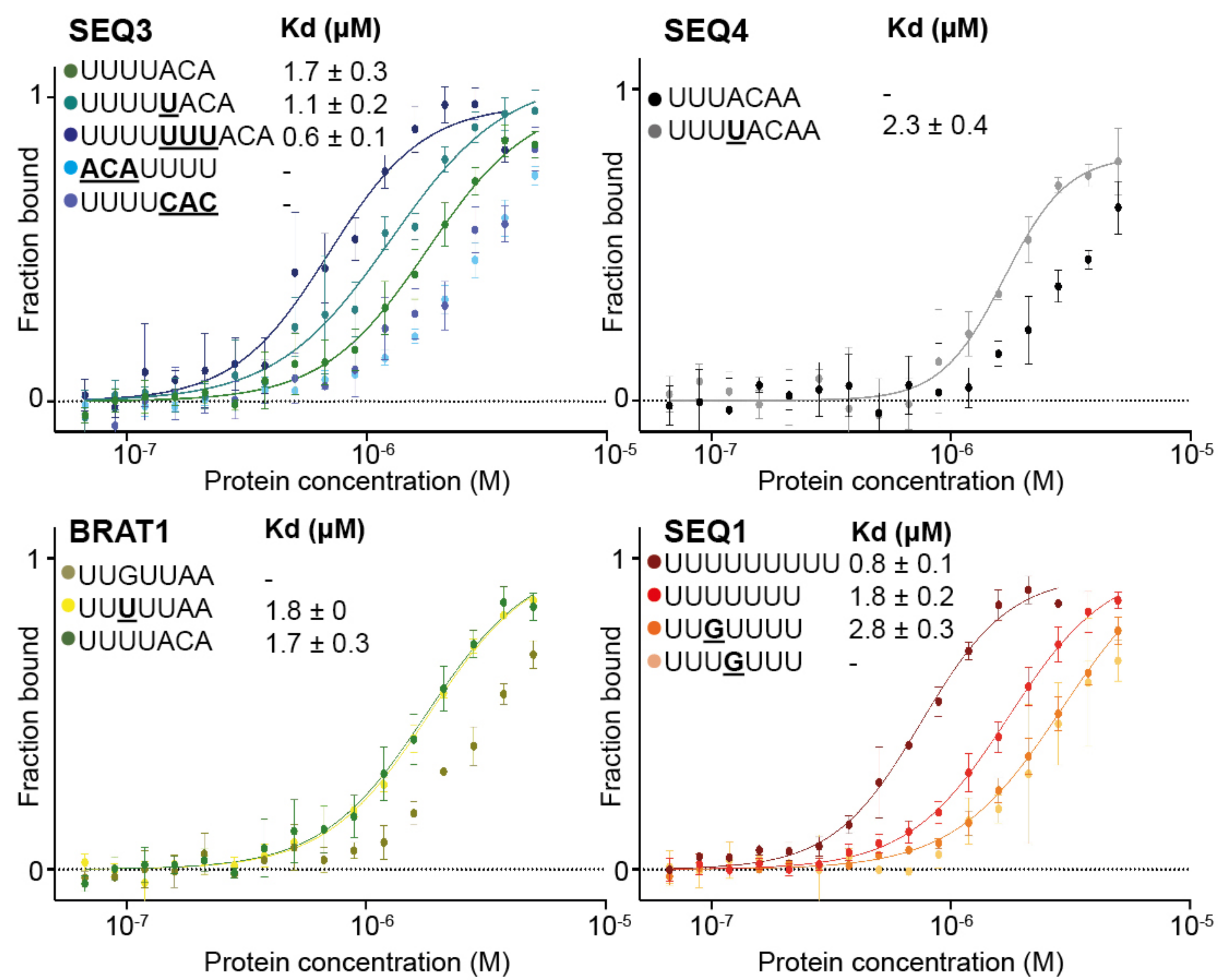
**B****C**

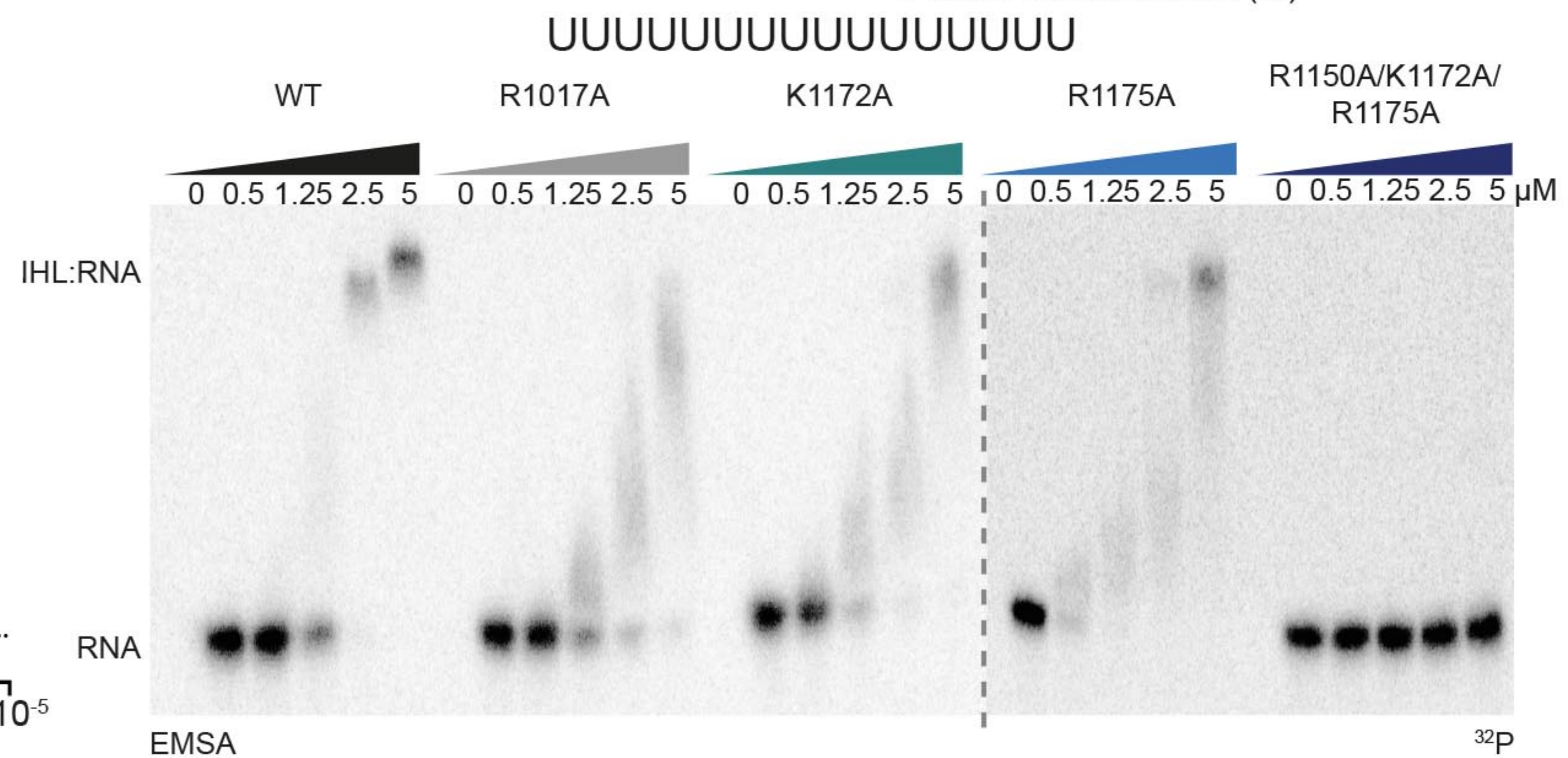
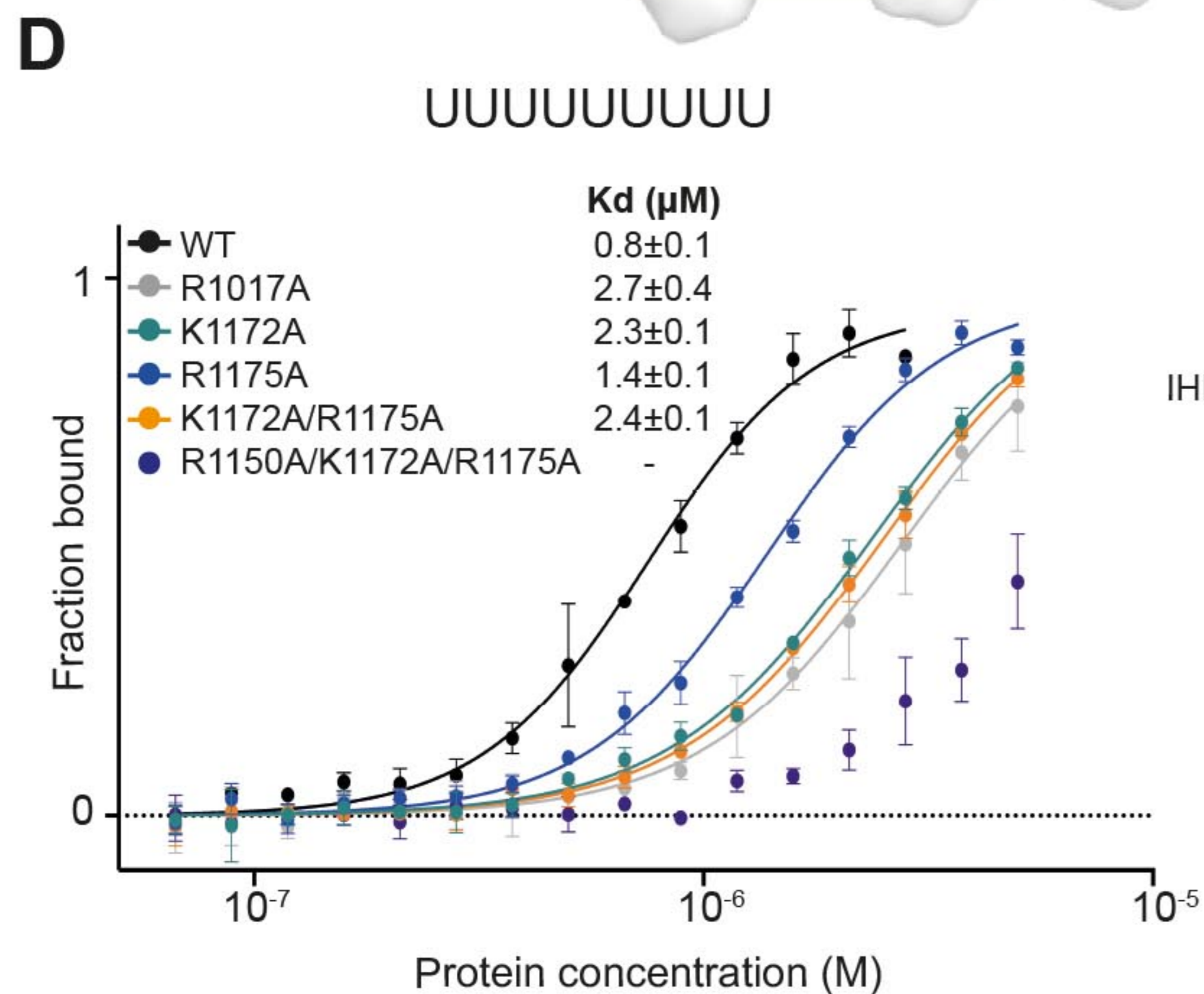
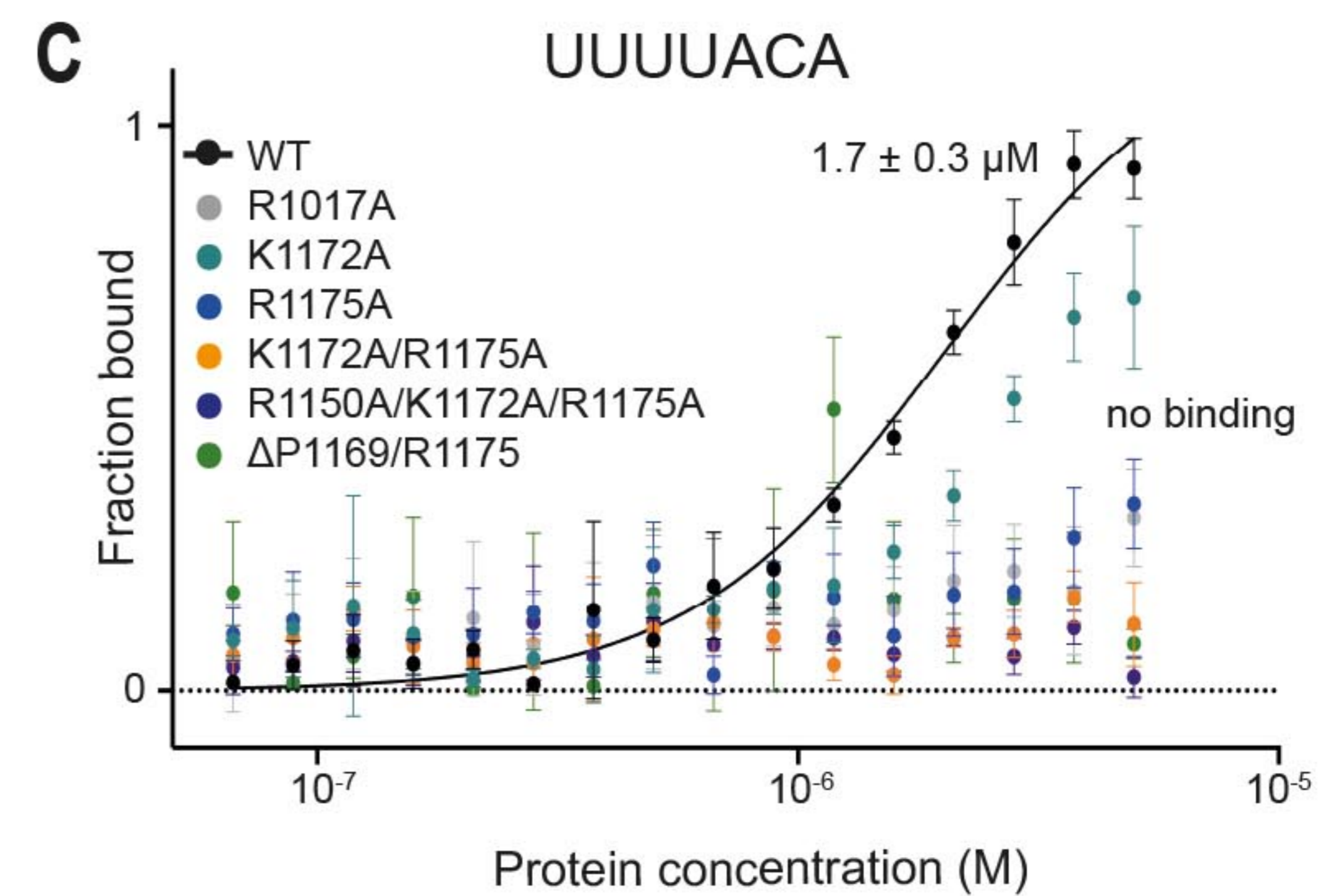
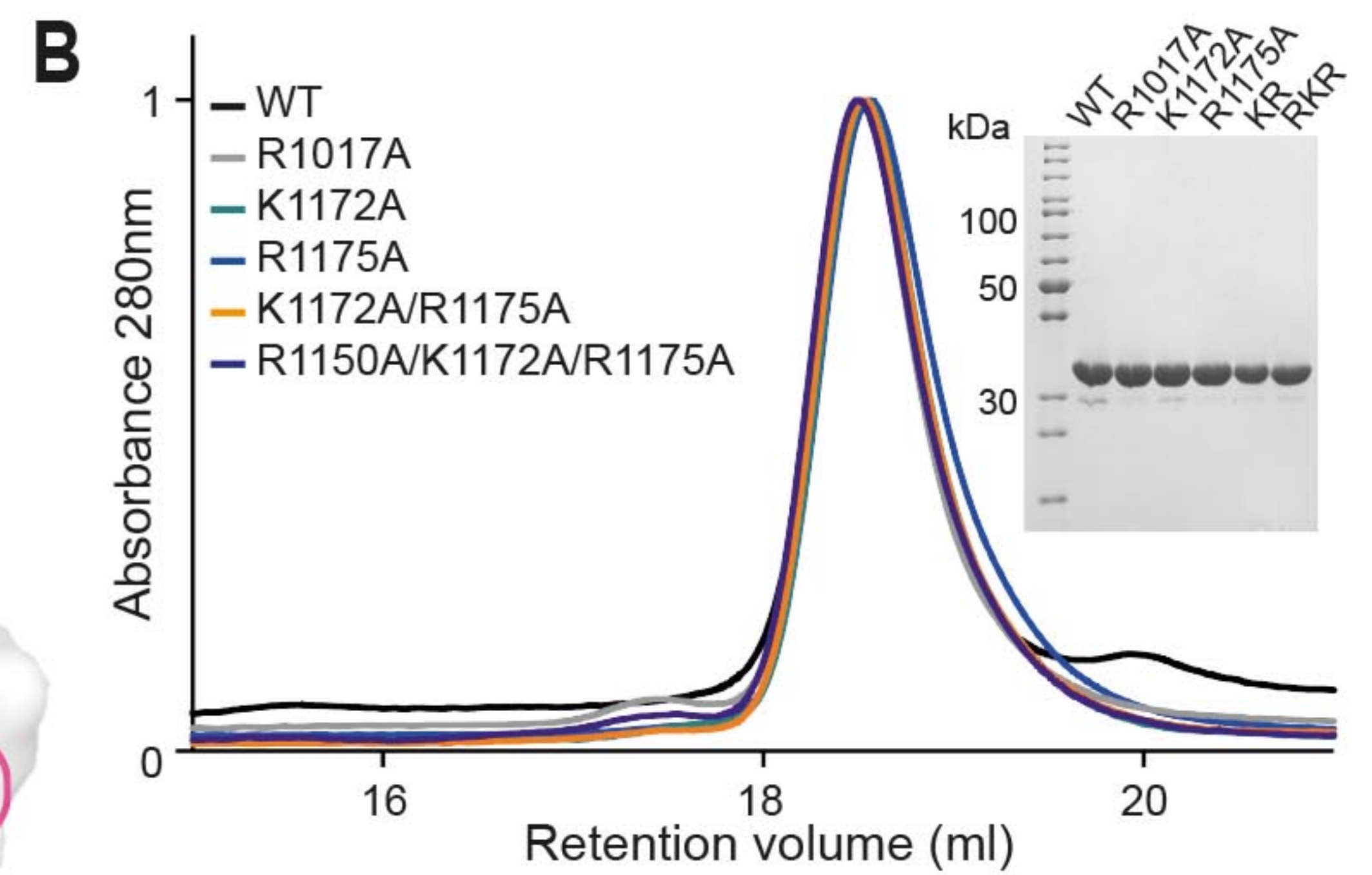
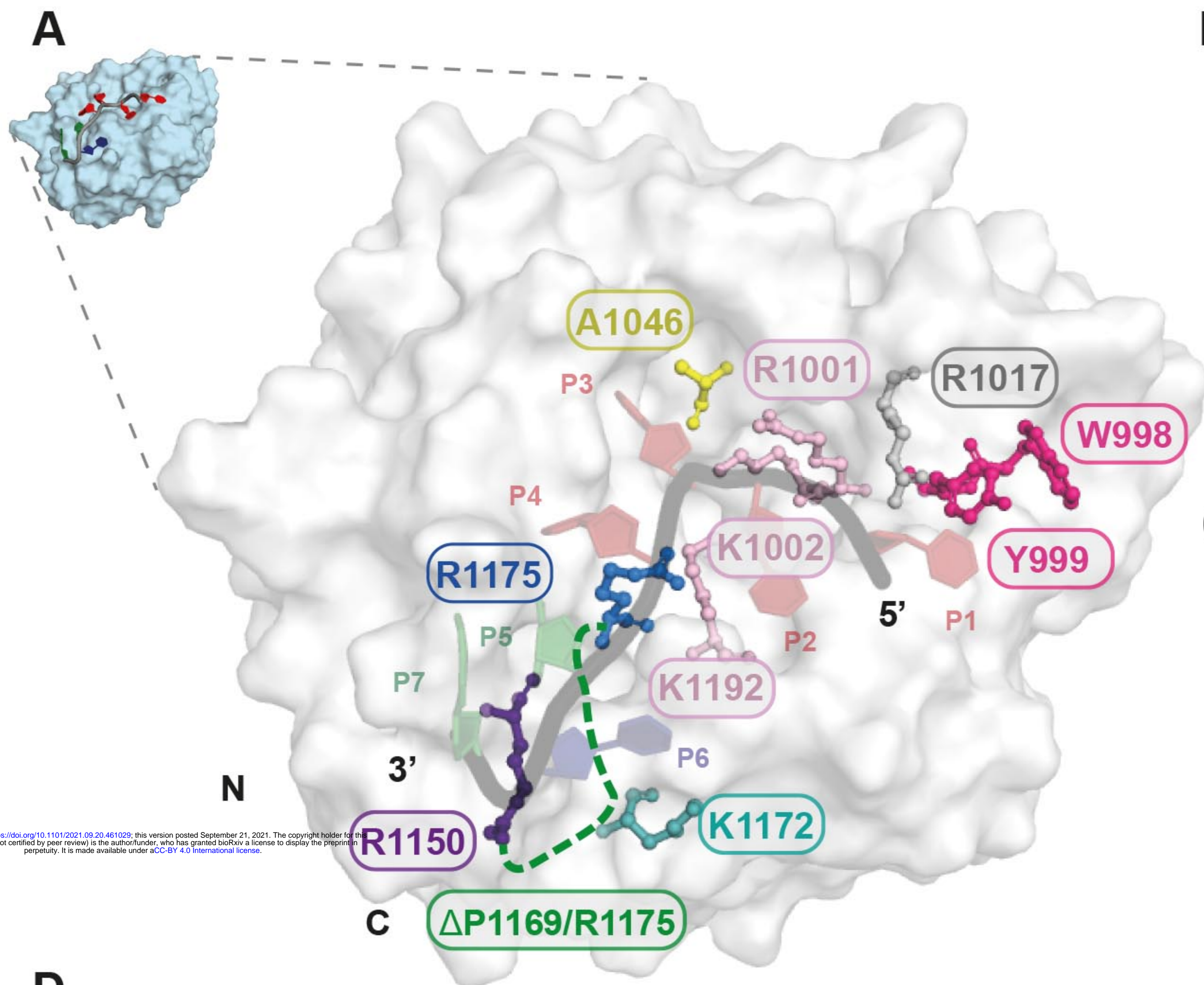
A**B**

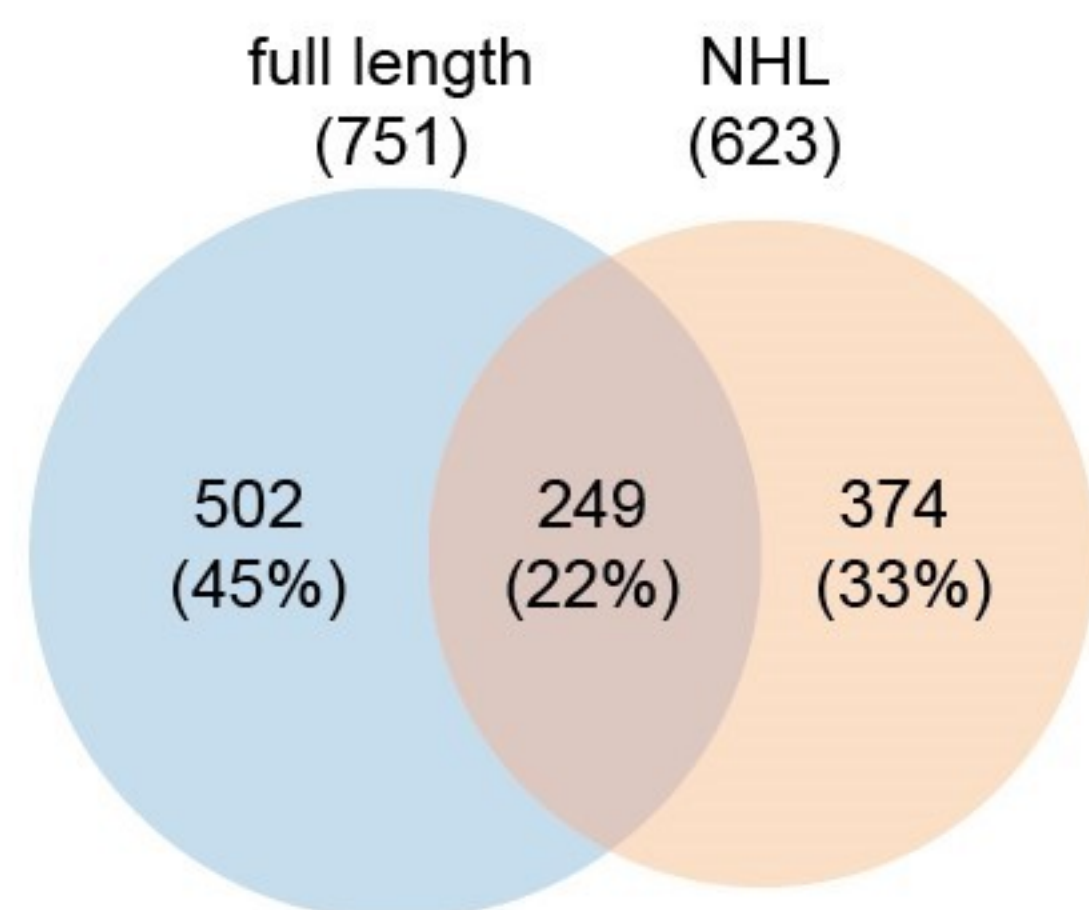
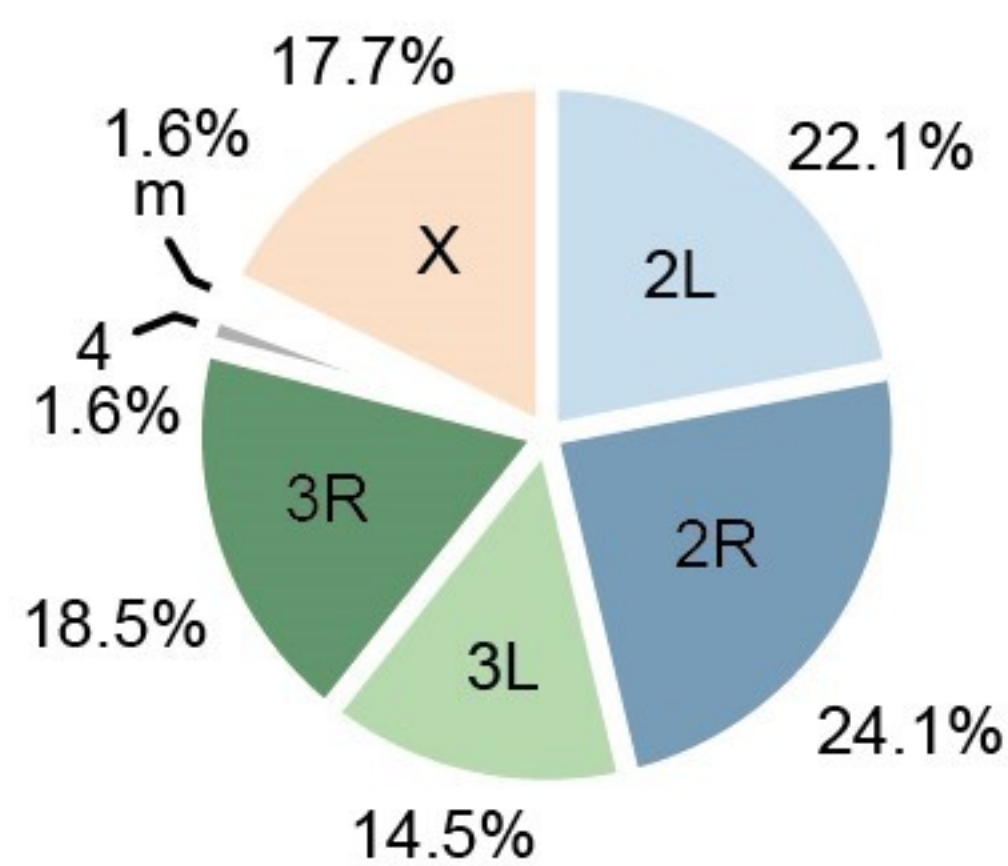
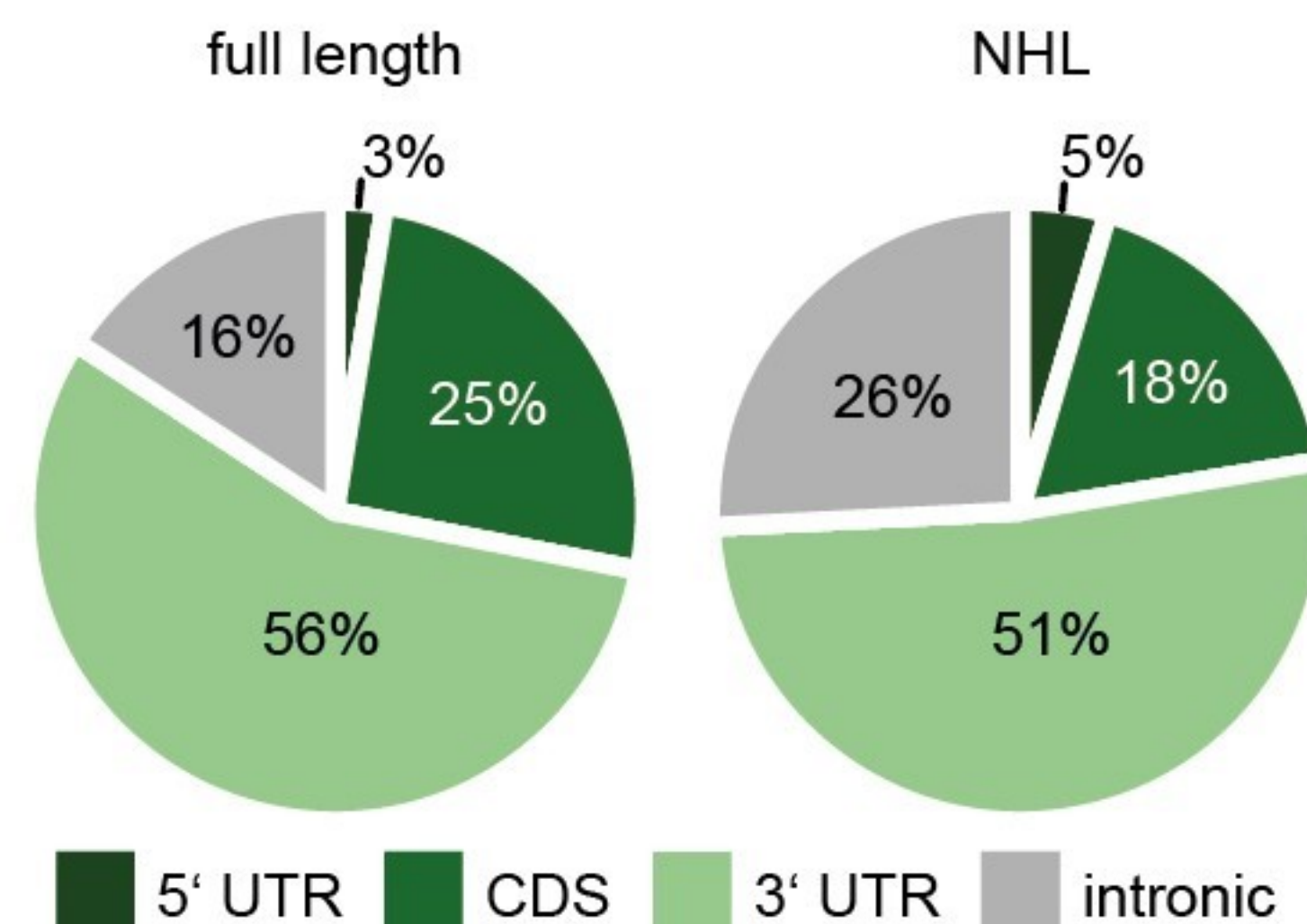
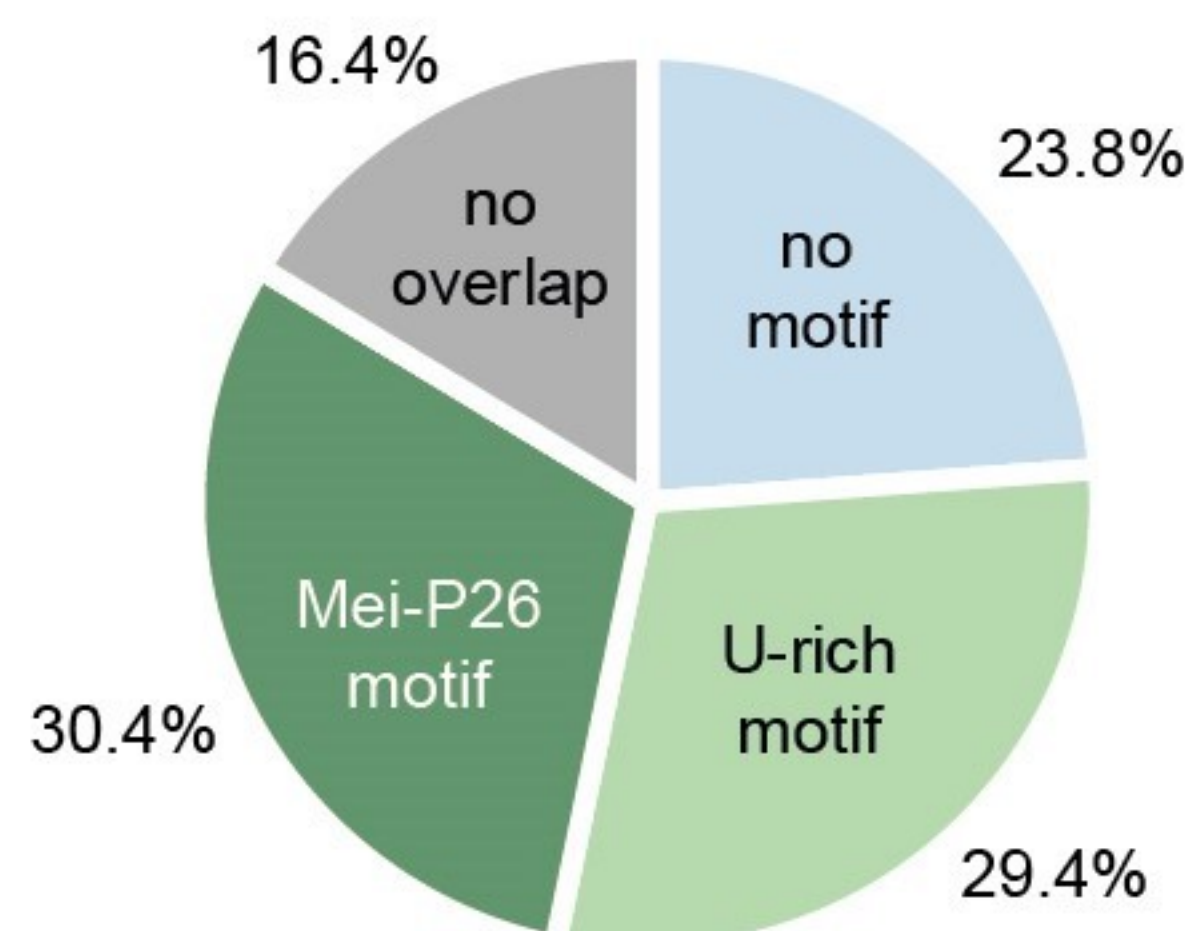
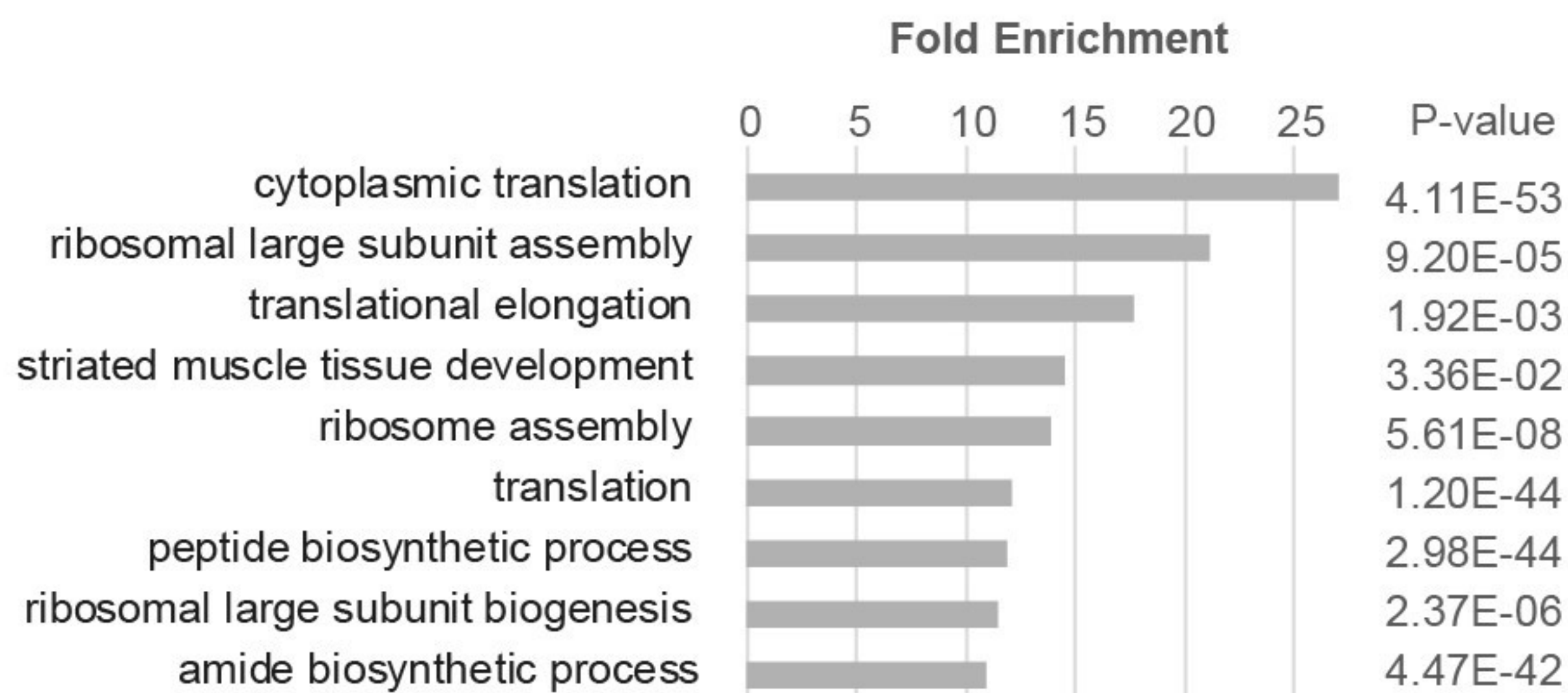
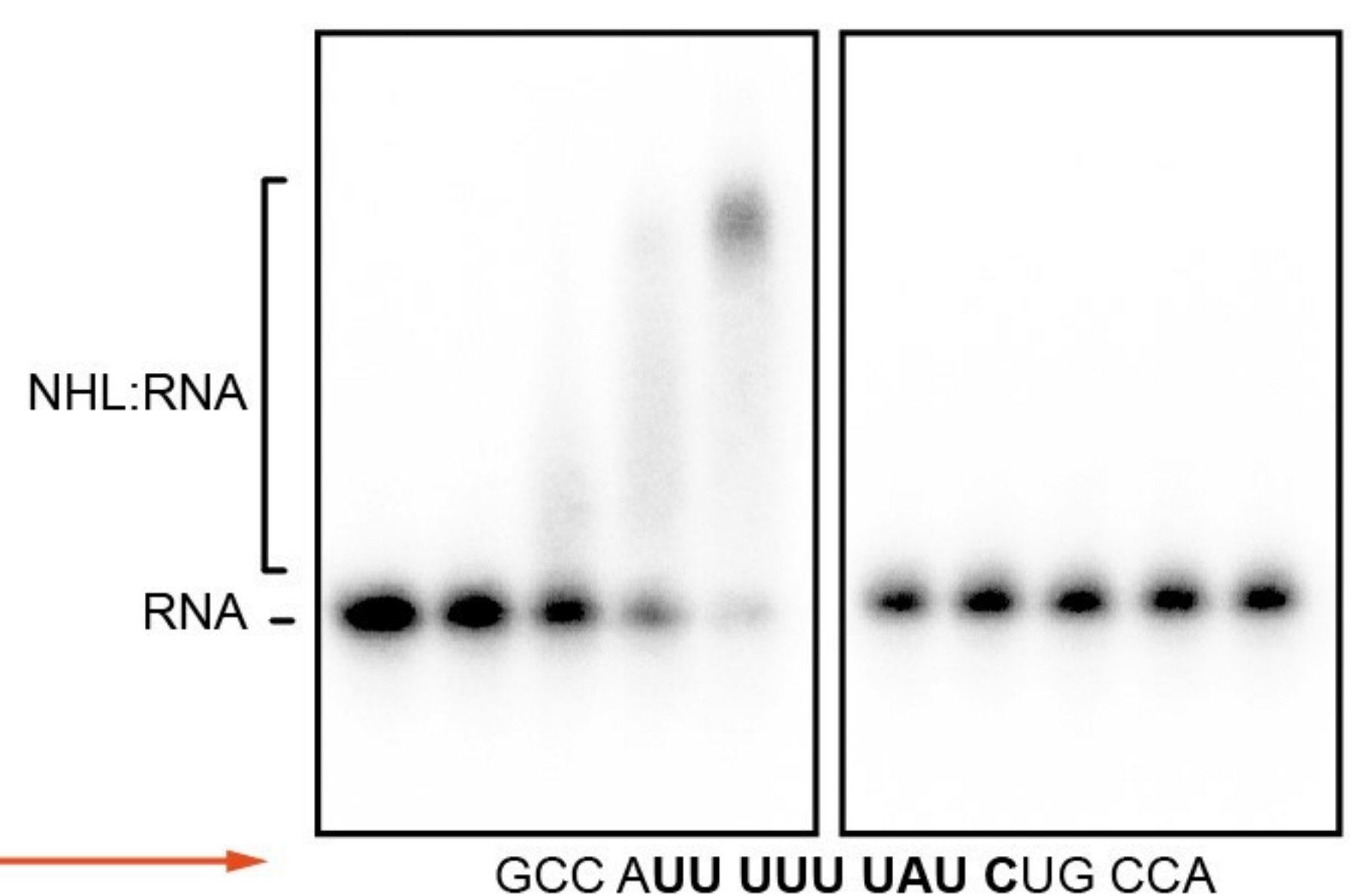
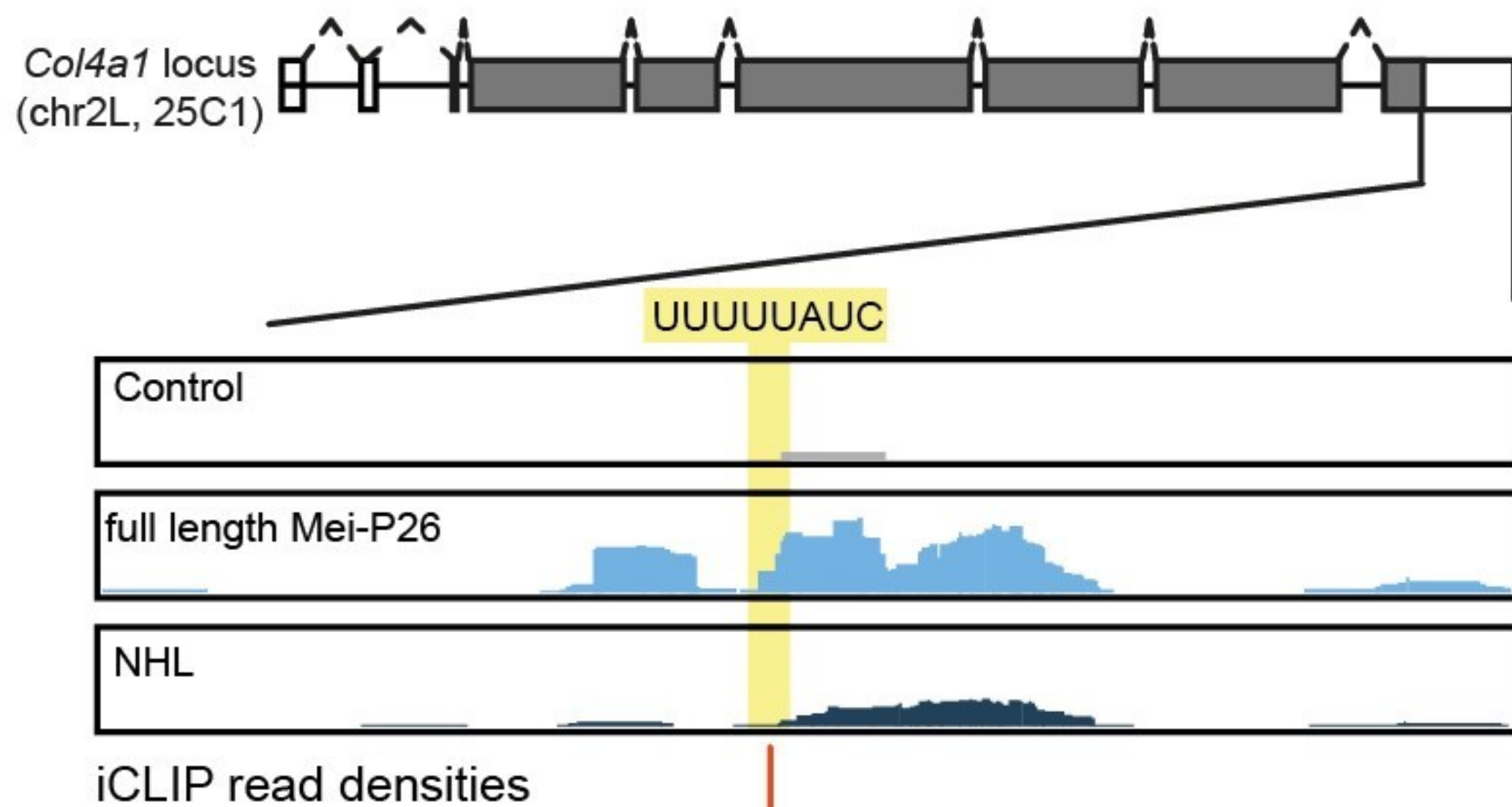
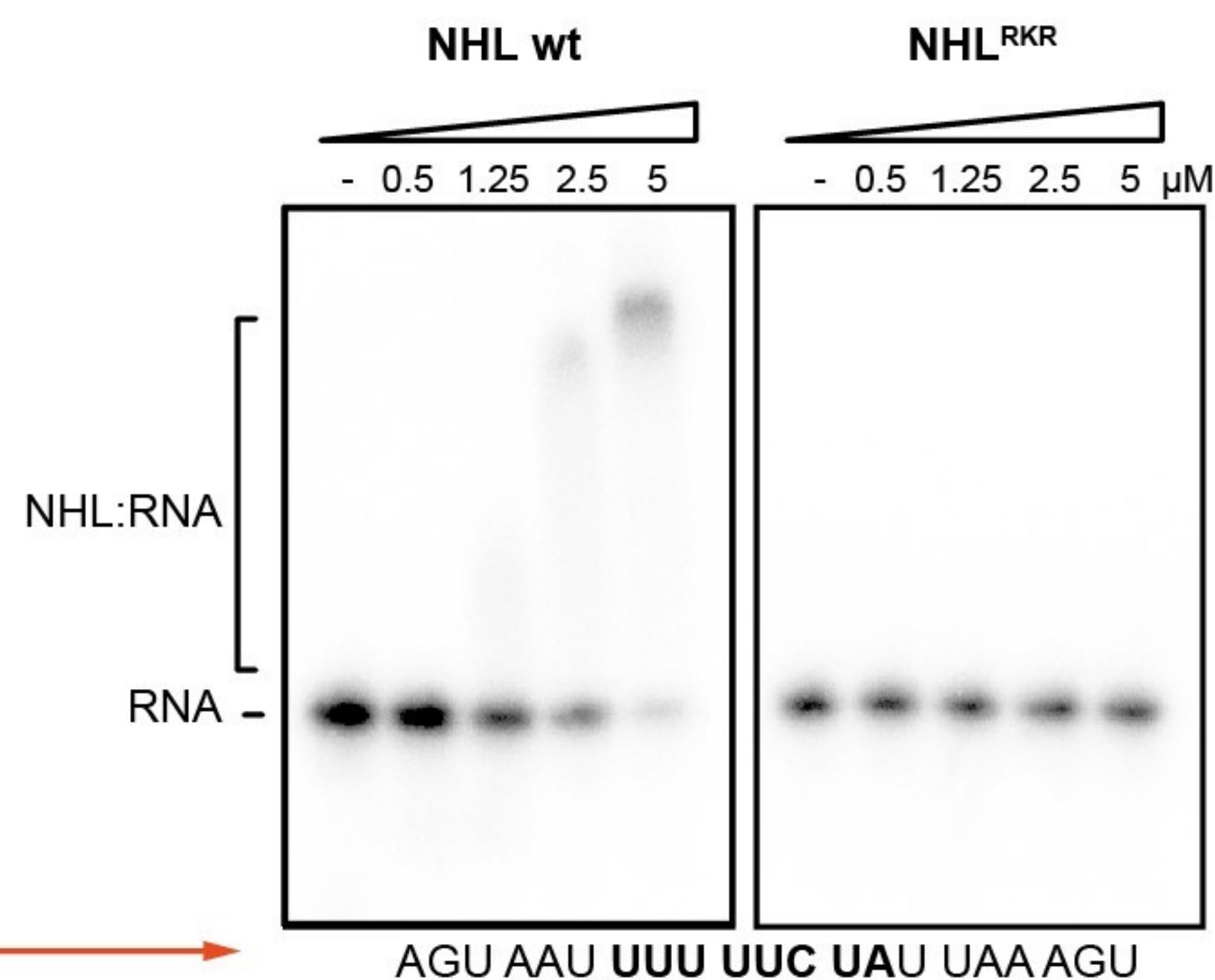
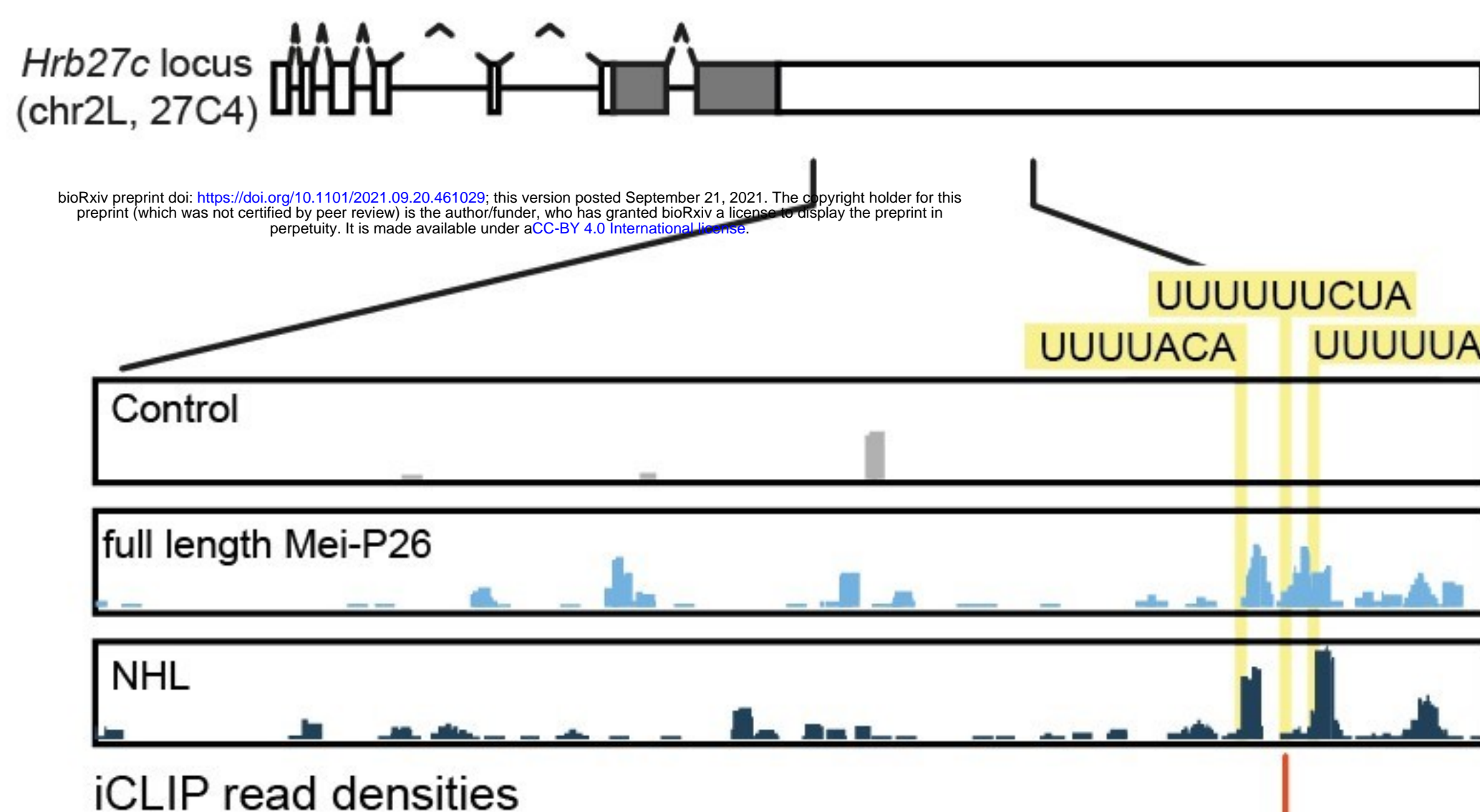
Mei-P26 NHL
5' UUUUACA 3'

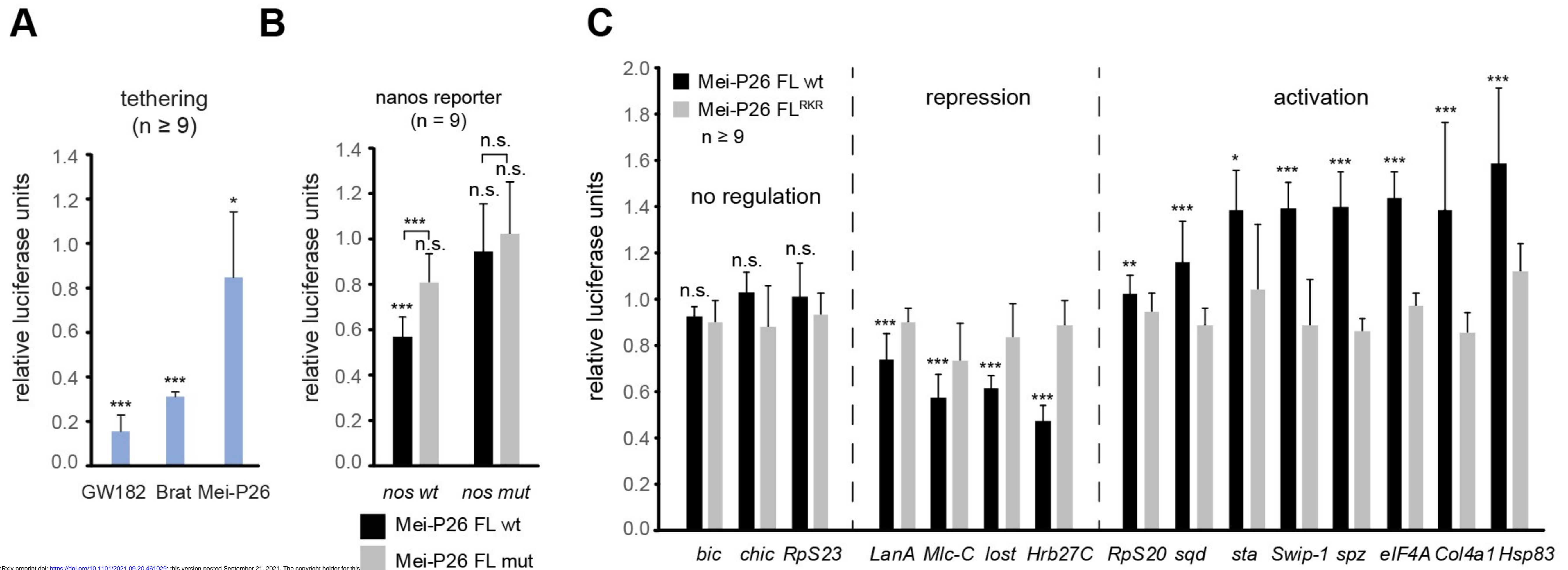


Mei-P26 NHL
5' UUUUUUUU 3'

**C****D**



A**B****C****D****E****F**



bioRxiv preprint doi: <https://doi.org/10.1101/2021.09.20.461029>; this version posted September 21, 2021. The copyright holder for this preprint (which was not certified by peer review) is the author/funder, who has granted bioRxiv a license to display the preprint in perpetuity. It is made available under aCC-BY 4.0 International license.

